Journal of Hazardous Materials 445 (2023) 130557

Contents lists available at ScienceDirect

Journal of Hazardous Materials

journal homepage: www.elsevier.com/locate/jhazmat

Unlocking the bentonite microbial diversity and its implications in selenium bioreduction and biotransformation: Advances in deep geological repositories

Cristina Povedano-Priego [a], Fadwa Jroundi [a,*], Pier L. Solari [b], Isabel Guerra-Tschuschke [c], María del Mar Abad-Ortega [c], Alexander Link [d], Ramiro Vilchez-Vargas [d], Mohamed L. Merroun [a]

[a] Department of Microbiology, Faculty of Sciences, University of Granada, Granada, Spain
[b] MARS Beamline, Synchrotron SOLEIL, L'Orme des Merisiers, Saint-Aubin, Gif-sur-Yvette Cedex, France
[c] Centro de Instrumentación Científica (CIC), University of Granada, Granada, Spain
[d] Department of Gastroenterology, Hepatology and Infectious Diseases, University of Magdeburg, Magdeburg, Germany

HIGHLIGHTS

- Bioreduction of Se(IV) to Se(0) occurred in a complex bentonite-bacteria system.
- Allotropic biotransformation of amorphous Se(0) to trigonal Se(0) was achieved.
- Enrichment of indigenous bacteria involved in Se cycle enhanced its immobilization.
- These findings highlight the bacterial interactions with toxic forms of selenium.

GRAPHICAL ABSTRACT

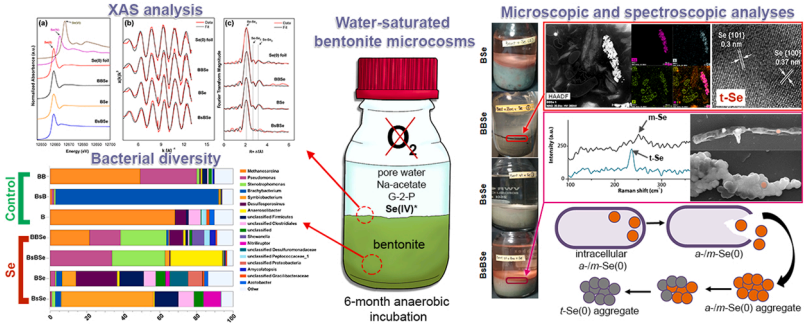

ARTICLE INFO

Editor: Debora F. Rodrigues

Keywords:
Selenite
Bentonite microcosms
Microbial community
Biotransformation
DGR

ABSTRACT

Selenium, ^{79}Se, is one of the most critical radionuclides in radioactive waste disposed in future deep geological repositories (DGRs). Here, we investigate the impact of bentonite microbial communities on the allotropic transformation of Se(IV) bioreduction products under DGR relevant conditions. In addition, Se amendment-dependent shifts in the bentonite microbial populations are assessed. Microcosms of water-saturated bentonites were spiked with a bacterial consortium, treated with selenite and incubated anaerobically for six months. A combination of X-Ray Absorption Spectroscopy, Electron Microscopy, and Raman Spectroscopy was used to track the allotropic changes of the Se bioreduction products. Interestingly, the color of bentonite shifted from orange to black in the selenite-treated microcosms. In the orange layers, amorphous or monoclinic Se(0) were identified, whilst black precipitates consisted of stable trigonal Se(0) form. Illumina DNA sequencing indicated the distribution of strains with Se(IV) reducing and Se(0) allotropic biotransformation potential, like *Pseudomonas*, *Stenotrophomonas*, *Desulfosporosinus*, and unclassified-*Desulfuromonadaceae*. The archaea *Methanosarcina*

* Correspondence to: Department of Microbiology, Faculty of Sciences, University of Granada, Campus Fuentenueva s/n 18071, Granada, Spain.
E-mail addresses: ppriego@ugr.es (C. Povedano-Priego), fadwa@ugr.es (F. Jroundi), pier-lorenzo.solari@synchrotron-soleil.fr (P.L. Solari), iguerra@ugr.es (I. Guerra-Tschuschke), mmabad@ugr.es (M.M. Abad-Ortega), alexander.link@med.ovgu.de (A. Link), ramiro.vilchez@med.ovgu.de (R. Vilchez-Vargas), merroun@ugr.es (M.L. Merroun).

https://doi.org/10.1016/j.jhazmat.2022.130557
Received 12 September 2022; Received in revised form 28 November 2022; Accepted 3 December 2022
Available online 5 December 2022

decreased its abundance in the presence of Se(IV), probably caused by this oxyanion toxicity. These findings provide an understanding of the bentonite microbial strategies involved in the immobilization of Se(IV) by reduction processes, and prove their implication in the allotropic biotransformation from amorphous to trigonal Se(0) under DGR relevant conditions.

1. Introduction

Deep Geological Repository (DGR) is the internationally accepted option for the storage and management of high-level radioactive waste (HLW) (Grigoryan et al., 2018). This multi-barrier system consists of encapsulating spent fuel in metal canisters surrounded by an engineered barrier (e.g., highly compacted bentonite) and emplaced deeply within a host rock (natural geological barrier) (Anderson et al., 2011; Bengtsson and Pedersen, 2017). All evolution scenarios of nuclear waste disposal suggest that the release of radionuclides over a long-term period in the repository would be unavoidable.

Among the radionuclides generated by nuclear fuel reprocessing activities, the isotope ^{79}Se is a critical one occurring in the HLW, turning it problematic in the DGR systems (Kang et al., 2011). The principal production of selenium-79 is the nuclear fission generating a cumulated fission yield of 0.049%. In addition, its long half-live, beside that of a few other radionuclides, determines the radiological impact in the DGRs (Jörg et al., 2010). The toxicity of selenium is mainly related to the oxidation state, being Se oxyanions (selenate [Se(VI)] and selenite [Se (IV)]) the most toxic forms for their high solubility and mobility causing harmful effects in the environment (Avendaño et al., 2016; Garbisu et al., 1996; Nancharaiah and Lens, 2015). In turn, elemental selenium [Se(0)] and selenides [Se(-II)] are the less soluble and immobile, exhibiting thus low or no toxicity in the terrestrial and aquatic environments (Avendaño et al., 2016). Therefore, it is necessary to study the biotic and abiotic processes that could influence the fate and mobility of such metalloid under DGR relevant conditions, where anaerobic and reducing environments will be prevalent over a long period of time.

In the DGRs, bentonite has been selected as the engineered barrier because of its suitable properties including the capacity of radionuclide retardation, mainly provided by the composition in montmorillonite (Montavon et al., 2009). Montavon et al. (2009) reported the key role that montmorillonite plays in controlling the sorption of Se(IV) in bentonites at pH above 7. Reduction of Se(IV) to Se(0) by pyrite (FeS_2) is another selenite immobilization mechanism (Han et al., 2012; Kang et al., 2011). In bentonites, Se(IV) reduction by pyrite seems to be preceded by mineral surface adsorption of selenite, which is afterwards reduced to poorly soluble Se(0) or $FeSe_2$ (Hoving et al., 2019). In addition to these abiotic factors, it has been reported that microbes can interact with this metalloid through different processes such as reduction (Ruiz-Fresneda et al., 2019, 2018), oxidation (Eswayah et al., 2016; Nancharaiah and Lens, 2015), and volatilization (Ansede and Yoch, 1997, 2020), affecting thus its speciation and in consequence its mobility in the environment. In recent years, bentonites showed to contain high diversity and activity of microorganisms (Grigoryan et al., 2018; Lopez-Fernandez et al., 2018, 2015, 2014; Povedano-Priego et al., 2022, 2021, 2019), which could interact with Se. For instance, *Stenotrophomonas bentonitica*, isolated from Spanish bentonite, was able to tolerate up to 200 mM of selenite reducing it to Se(0) (Ruiz-Fresneda et al., 2018). Different mechanisms have been described to explain this bioreduction, such as the intracellular reduction mediated by molecules containing reduced thiol groups (-SH) (Li et al., 2014) or by reductase enzymatic activity (Basaglia et al., 2007; Hunter, 2014; Li et al., 2014; Pinel-Cabello et al., 2021). However, the DGR conditions would result in a very harsh and complex environment for microorganisms to develop their growth and activities (Povedano-Priego et al., 2021). This environment involves low water and nutrients availability, low physical space (average pore diameter of 0.02 μm), high swelling pressures in the order of 7–8 MPa at full water saturation, anoxic atmosphere, and high temperatures and radiation. Thus, it is crucial to study the potential viability and activity of microorganisms inhabiting the bentonite within the context of a DGR system (Beaver et al., 2022; Povedano-Priego et al., 2021).

Se(0) prevails in anaerobic conditions and may exist in different allotropic forms as amorphous (*a*-Se), monoclinic (*m*-Se), and trigonal (*t*-Se) (Chen et al., 2010; Nancharaiah and Lens, 2015). Several bacteria, such as *Shewanella* spp. and *Stenotrophomonas* spp., have been reported to produce *a*-Se(0) (Ruiz-Fresneda et al., 2018; Tam et al., 2010). Others like *Ralstonia metallidurans* can reduce Se(IV) forming intracellular *m*-Se (Oremland et al., 2004; Sarret et al., 2005). The latter is metastable and could also eventually suffer a conversion to the *t*-Se form (Goldan et al., 2016). Besides, these *m*-Se nanostructures can be found in three different allotropes (alpha, beta and gamma) composed by 8 atoms of Se in polymer rings (Fernández-Martínez and Charlet, 2009). In turn, the *t*-Se is composed of polymeric helical chains of Se atoms parallel to each other, where every atom is connected by partially metallic bonds with four nearby Se atoms in the adjacent chains. Such structure confers to the *t*-Se a high stability, in contrast to the weaker van der Waals forces linking the Se atoms in the *m*-Se (Fernández-Martínez and Charlet, 2009; Goldan et al., 2016). Biotransformation of *a*-/*m*-Se into the most stable trigonal form could be undertaken by several bacterial strains such as *S. bentonitica* and *Bacillus subtilis* (Ruiz-Fresneda et al., 2018; Wang et al., 2010).

The significant impact of the microbial processes on the mobilization/immobilization of radionuclides and the risk that Se may have on the safety of DGR are in the urgent need to be understood. Therefore, by using state-of-the-art microscopic and spectroscopic techniques, this work aims to 1) investigate the potential effect of Se(IV) on the microbial community of bentonite, 2) identify tolerant bacterial strains involved in the transformation of the toxic Se(IV) into the less-toxic Se(0), and 3) determine the impact of bentonite microbial community on the structure and chemical speciation of Se(IV) reduction products, in a complex system of water-saturated bentonite amended with selenite and a bacterial consortium, described by their capacity to interact with radionuclides (e.g., uranium and selenium).

2. Materials and methods

2.1. Bentonite collection and water-saturated bentonite microcosms preparation

2.1.1. Samples collection

Bentonite samples were collected from the clay formation in "El Cortijo de Archidona" (Almeria, Spain) in January 2018, under aseptic conditions in previously sterilized containers and then stored at 4 ºC until further use.

2.1.2. Preparation of the different solutions

Pore water (PW) for bentonite saturation was extracted by shaking 1 g of bentonite in 100 mL of sterile distilled water at 180 r.p.m. for 24 h at 28 ºC. Then, the aqueous phase was filtered using 0.45 μm pore-size sterile filters and autoclaved twice at 110 ºC for 20 min. The composition of major elements of this PW was previously described in Povedano-Priego et al. (2019). PW was supplemented with 30 mM sodium acetate and 10 mM glycerol-2-phosphate (G2P) as electron donors to stimulate the growth of bentonite bacterial communities.

For the interaction with Se experiments, a stock solution of 1 M sodium selenite (Na_2SeO_3; Sigma-Aldrich) was prepared and sterilized by

filtration in 0.22 μm pore-sized syringe filters (Sartorius).

2.1.3. Bacterial strains and growth conditions

In this study, a consortium composed of five bacterial strains, previously detected in the microbial community of Spanish bentonite (Lopez-Fernandez et al., 2018, 2014; Povedano-Priego et al., 2021, 2019), was added to the water-saturated microcosms. This consortium consisted of *Stenotrophomonas bentonitica* BII-R7^T and *Bacillus* sp. BII-C3, both of which were previously isolated from Spanish bentonite (Lopez-Fernandez et al., 2014). In addition, *Pseudomonas putida* ATCC33015, *Amycolatopsis ruanii* NCIMB14711, and *Shewanella loihica* DSM17748 were purchased from the culture collections: ATCC (American Type Culture Collection; https://www.lgcstandards-atcc.org/), NCIMB (National Collection of Industrial Food and Marine Bacteria; https://www.ncimb.com/), and DSMZ (Deutsche Sammlung Von Mikroorganismen Und Zellkulturen; https://www.dsmz.de/), respectively. This consortium hereinafter will be referred to as BSPAS. All bacterial strains were grown aerobically in Luria-Bertani (LB) broth medium (tryptone 10 g L^{-1}, yeast extract 5 g L^{-1}, and NaCl 10 g L^{-1}), except *A. ruanii* that was grown in yeast-malt broth (yeast extract 4 g L^{-1}, malt extract 10 g L^{-1}, glucose 4 g L^{-1}). Initial Optical Density for each bacterium was adjusted to 0.4 at 600 nm (OD_{600}) (Genesys 10 S UV-Vis; Thermo scientific, MA, USA), before used in the bacterial consortium-containing treatments.

2.1.4. Experimental set-up

Water-saturated microcosms were prepared in sterile 250-mL borosilicate glass bottles, consisting of 40 g of ground bentonite and 170 mL of PW, glycerol-2-phosphate (G2P) and sodium acetate solutions reaching a final volume of 230 mL. In the case of selenite-treated microcosms, 1 M sodium selenite solution was added to a final concentration of 2 mM. Finally, the bentonite microcosms were spiked with the BSPAS consortium. The microcosms preparation is illustrated in Fig. 1. Different controls were performed such as 1) without any spiked bacteria, 2) with no Se, and 3) using bentonite "sterilized" by tyndallization (100 ºC for 30 min during 3 consecutive days), referred in the text as sterile bentonite. In total, 8 different treated microcosms were prepared: BBSe (Bentonite spiked with BSPAS and Selenite); BB (Bentonite with BSPAS); BsBSe (Bentonite, sterile, spiked with BSPAS and Selenite); BsB (Bentonite, sterile, spiked with BSPAS); BSe (Bentonite treated with Selenite); B (Bentonite); BsSe (Bentonite, sterile, treated with Selenite); Bs (Bentonite, sterile). Each treatment was prepared in triplicate (3 replicates each), obtaining 24 samples for all the experiment. These experimental conditions are detailed in Supplementary Table S1.

The 250-mL borosilicate glass bottles were sealed with the butyl-rubber stoppers (Supplementary Fig. S1A) and bubbled with N_2 (for ~20 min each) until saturation to create anaerobic conditions (Supplementary Fig. S1B). Afterwards, microcosms were incubated for six months at room temperature (Fig. 1).

2.2. Chemical characterization of the supernatant from water-saturated microcosms

The pH of all 24 supernatant was measured from the water-saturated microcosms using Advanced Digital Handheld Portable Meter HQ40D (Hach), calibrated against pH 4.00 and 7.02 commercial reference solutions.

Determination of selenium concentration in the supernatants was carried out using Inductively Coupled Plasma-Mass Spectrometry (ICP-MS) using NexION 300D spectrometer. The measurements were performed at time 0, and after 3, and 6 months of anaerobic incubation.

2.3. Mineralogical and microscopic characterization of water-saturated bentonite microcosms and selenium nanoparticles (SeNPs)

Se-treated microcosm samples were analyzed by Variable Pressure

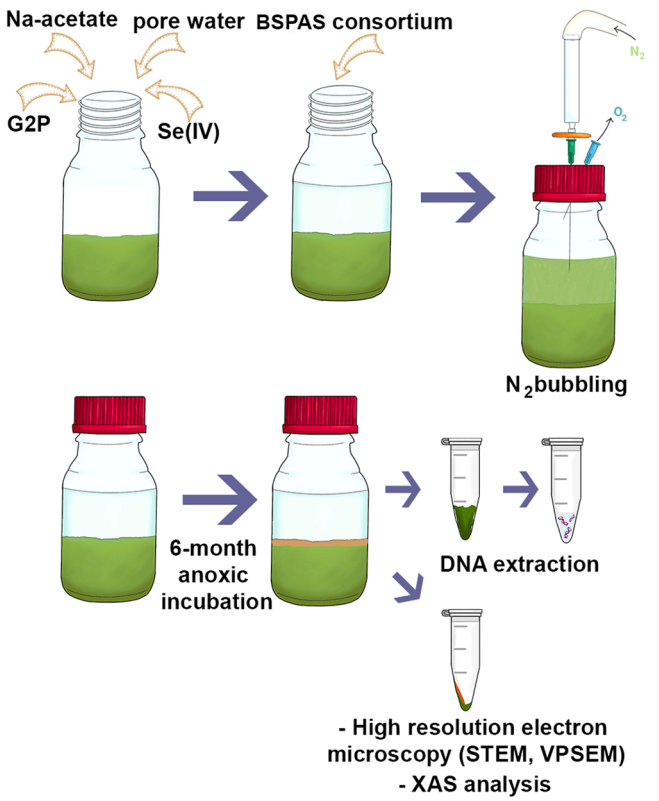

Fig. 1. Workflow of the microcosm set-up, and the nitrogen bubbling resulting in anaerobic conditions after the 6-month incubation period. Water-saturated bentonites were used for DNA extraction, and the interface for High Resolution Transmission and Scanning Electron Microscopy, and X-ray absorption spectroscopy (XAS) analysis.

Field Emission Scanning Electron Microscopy (VP-FESEM) *ZeissSupra 40VP* equipped with secondary electron (SE) and backscattered electron (BSE) detectors. This microscope is coupled with a microanalysis system (*Aztec 2.2*) to deliver elemental composition data by Energy Dispersive X-ray (EDX) and equipped with Raman spectrometer *Renishaw In Via* fitted with a Nd:YAG 532 nm laser and a near-infrared diode 785 nm laser, with 500 mW and 100 mW as maximum powers, respectively (Guerra and Cardell, 2015).

Additional ultrastructural features on the SeNPs and water-saturated bentonite were determined using Scanning Transmission Electron Microscope (STEM; FEI TITAN G2 80–300) equipped with an EDX spectrometer working at 300 kV and a High-Angle Annular Dark Field (HAADF) detector. The characterization of Se nanoparticles was performed by Selected-Area Electron Diffraction (SAED) and High-Resolution Transmission Electron Microscopy (HRTEM) combined with Fast Fourier Transform (FFT). Samples were prepared as described in Povedano-Priego et al. (2019).

2.4. X-ray Absorption Spectroscopy (XAS) analysis of the Se-bentonite samples

For XAS experiments the supernatant layers of the Se(IV)-amended bentonites microcosmos samples were collected, dried, and powdered. The powdered samples were prepared by spreading and pressing them onto 10 mm × 3 mm area of Kapton tape, which was sealed between additional layers. Selenium references (sodium selenate (Se^{VI}), sodium selenite (Se^{IV}) and Se^0 foil) were prepared as it was described in Ruiz-Fresneda et al. (2020). Their XAS data were collected in transmission mode.

Se K–edge XAS of the studied samples were collected at the MARS beamline at the SOLEIL synchrotron facility, which is the French

bending magnet beamline dedicated to Multi Analyses on radioactive materials (Sitaud et al., 2012). For the experiment, the ring was operated at 2.75 GeV in 8-bunch mode (100 mA). The optics consisted on a double-crystal monochromator with horizontal dynamical focusing set to the Si (220) crystals, and -coated mirrors for vertical focusing and rejection of higher harmonics set to the Si strips (Solari et al., 2009). Spectra were collected in fluorescence mode using a 13-element Ge detector (EG & G ORTEC, USA). Data were processed following standard procedures by using the Athena codes (Ravel and Newville, 2005). Background removal was performed by means of a pre-edge linear function. Atomic absorption was simulated with a square-spline function. The theoretical phase and amplitude functions used in data analysis were calculated with FEFF8 (Ankudinov et al., 1998) using the trigonal Se as atomic model. The amplitude reduction factor ($S0_2$) was held constant at 1.0 for the FEFF8 calculation and Extended X-ray Absorption Fine Structure (EXAFS) fits. The shift in threshold energy, ΔE_0, was varied as a global parameter in the fits. The absorption threshold E_0 was set to 12,658 eV using the peak of the first derivative near the absorption edge. Fitting was performed in R-space with a k-weight of 3. A k range of 4–13 $Å^{-1}$ was used for the $|\chi(R)|$ transform.

2.5. Characterization of the bentonite bacterial community in the water-saturated microcosms

2.5.1. DNA extraction from bentonite microcosms

DNA extraction from all treated microcosms was performed as described in detail in Povedano-Priego et al. (2021). Extracted DNA was stored at − 20 ºC until further used. DNA purification was performed with 0.1 volumes of 20% sodium acetate and 2.5 volumes of ice-cold absolute ethanol. The tubes were incubated at − 20 °C for one hour and then centrifuged at 12,000g for 10 min at 4 °C. The pellets were washed with 70% ethanol followed by centrifugation under the same conditions. Finally, pellets were air-dried to be then dissolved in MilliQ water.

2.5.2. Library preparation and sequencing

Two consecutive PCR reactions were performed for each sample with the use of normal and bar coded fusion primers for the library preparation. The primers used for amplification of V5-V6 variable regions of 16S rRNA gene were 807F (5′-GGATTAGATACCCBRGTAGTC-3′) and 1050R (5′-AGYTGDCGACRRCCRTGCA-3′) (Bohorquez et al., 2012). The first PCR reaction was performed as follows: one cycle at 95 °C for 15 min; 35 cycles at 98 °C for 10 s, 55 °C for 10 s, and 72 °C for 45 s; and a final extension step at 72 °C for 2 min. The same conditions were performed for the barcoding (the second PCR reaction) by applying only 10 PCR cycles. Electrophoresis was done to check the quality of the library product. Libraries were sequenced by MiSeq Illumina platform (2 × 250 bp, Hayward, California, USA) for generating the FastaQ files.

Raw sequences for this study were deposited in the NCBI sequence read archive (SRA) under the accession number PRJNA877829.

2.6. Computational processing of the bacterial diversity and biostatistical analyses

Analyses of all FastaQ files were achieved using dada2 package in R (www.r-project.org) resulting in a unique table containing the sequence reads and abundances of all microcosms samples. Normalization was performed using the "phyloseq" package returning 354 phylotypes. Sequence reads were assigned to a taxonomic affiliation based on the Bayesian classification, establishing 80% pseudo-bootstrap threshold. Relative abundances of phylum, class, order, family and genus were obtained by Explicet 2.10.5 software (Robertson et al., 2013).

Alpha diversity was calculated to the lowest sample size (1006) and bootstrapped 100 times. Specific differences in the bacterial community structure were further visualized in a heatmap using the heatmap.2 function in the R gplots v. 3.0.1.1 package (Warnes et al., 2019) including only taxa at $\geq$ 1% relative abundance in at least one sample. At the genus level, microbial community composition was analyzed using PAST3 v.3.18 and the output was visualized with Principal Components Analysis (PCA) and Principal Coordinate Analysis (PCoA).

Significant differences in taxa relative abundance ($p < 0.05$) between the different samples were determined using a one-way ANOVA test. In addition, a Tukey posthoc test was used to test for significant differences in relative taxa abundance ($p < 0.05$) between treatments for the total community.

3. Results

3.1. pH and soluble selenium measurements

The pH values of the supernatant in the water-saturated bentonite were slightly alkaline with values ranging from 7.5 to 8.5 at time 0. Along the incubation period, no significant differences in pH were observed among the treated microcosms (selenite-treated and controls) after 3, and 6 months of incubation (Supplementary Fig. S2A). The pH values ranged between 8 and 8.7, practically stable during the whole experiment.

The samples were also analyzed by ICP-MS, to determine the concentration of soluble Se(IV) in the supernatants at different incubation times (0, 3, and 6 months). At 24 h (time 0), the measured Se(IV) showed a concentration around 1.9 mM in all the samples (Supplementary Fig. S2B). However, the residual Se(IV) in solution depended on the treatments at 3, and 6 months of incubation. In the case of BBSe, Se(IV) was practically removed from the solution after 3 months. However, the selenite reducing rate decreased in BSe, BsBSe, and BsSe, being the lower removal rate that obtained in the BsSe microcosms with nearly 71.5% of Se remaining in the solution after 6 months. In addition, the effect of indigenous bacteria is higher than that of the bacterial consortium, since 14.5% of Se(IV) remained in BsBSe (sterile bentonite with BSPAS consortium) samples, in comparison with BSe samples showing no selenite in solution after incubation (Supplementary Fig. S2B). These findings indicate the crucial role of the bacteria in the reduction of Se(IV) and its immobilization to Se(0) since the highest Se removal rate occurred when indigenous bacteria were present, enhanced by the presence of BSPAS consortium.

3.2. Se(IV) reduction in water saturated anaerobic bentonites: macroscopic evidence

During the anaerobic incubation, changes in color in the Se(IV)-treated microcosms were observed as shown in Fig. 2. In the first week of incubation, no changes occurred in the BSe and BsSe samples (without bacterial consortium addition), whilst the liquid phases (supernatants) in the bacterial consortium inoculated samples (BBSe and BsBSe) turned orange, being more intense in BBSe microcosms. Over the incubation time, the liquid phases of the samples BBSe, BsBSe, and BSe turned uncolored and an orange layer appears after one month of incubation, forming a thicker layer at the interface supernatant/bentonite. At that time, no changes were observed in the sample BsSe. Interestingly, in BBSe samples the whole bentonite phase acquired an orange tone, which after two-month of incubation turned dark (gray) with an incipient black layer at the surface of the clay mineral and the orange tone remained in a thin layer. Meanwhile, BsSe microcosms exhibited a thin orange layer after six months of incubation. From two to six months, the pigmented layers (orange in BSe and BsBSe, and black/gray in BBSe) increased in thickness. Lastly, several spots appeared after one month in the bentonite of the BSe microcosms and their quantity and size increased throughout the incubation time (Fig. 2). The interface layers of the all-six-month microcosms were recovered and prepared for their microscopic analyses.

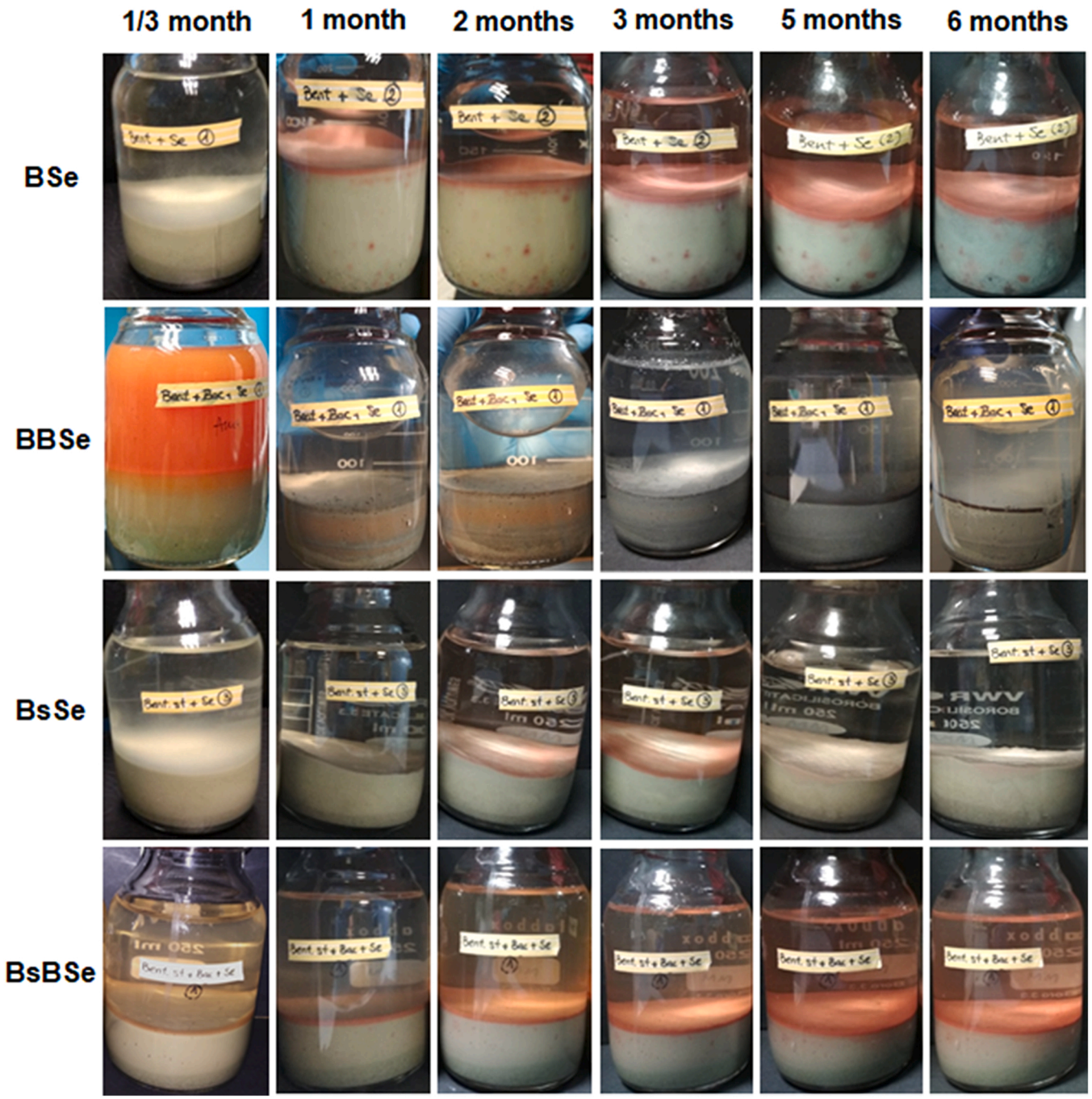

Fig. 2. Water-saturated bentonite microcosms treated with sodium selenite along the anaerobic incubation period (from 1/3–6 months). B=bentonite, Bs= bentonite (sterile), BB=bentonite spiked with BSPAS consortium, BsB= bentonite (sterile) spiked with BSPAS consortium, Se=sodium selenite treatment.

3.3. Microscopic (STEM/HAADF, VP-FESEM) and spectroscopic (Raman) characterization of the Se(IV) reduction products in water-saturated anaerobic microcosms

The interface orange layers of the 6 month-microcosms were recovered and prepared for their microscopic analyses. A combination of HAADF-STEM and VP-FESEM coupled with Raman spectroscopy were used to characterize the structure, morphology and element composition of Se(IV) reduction products. The crystalline structure of the SeNPs formed in Se-treated microcosms was determined by SAED and the lattice spacing measured using HRTEM combined with Fast Fourier Transform (FFT).

3.3.1. Bacterial consortium-spiked natural/sterile and Se(IV)-amended bentonite microcosms (BBSe and BsBSe)

HAADF-STEM micrographs of thin sections of the orange layer recovered from BsBSe and the black layer collected from BBSe showed the presence of electron-dense nanostructures of different shapes and sizes (Fig. 3). Intracellular nanostructures containing Se and S were observed in the thin section of the BsBSe microcosm, in addition to P arising from the cell biomass (Fig. 3a and b). SAED analyses determined that the SeNPs were crystalline (Fig. 3e). These SeNPs associated to the plasmatic membrane (Fig. 3e) were analyzed by HRTEM showing a lattice spacing of 0.33 nm corresponding to the (212) plane of *m*-Se (Fig. 3f). The most abundant SeNPs in the BsBSe microcosms were found inside the bacterial cells (Fig. 4a) or associated to cell debris or organic

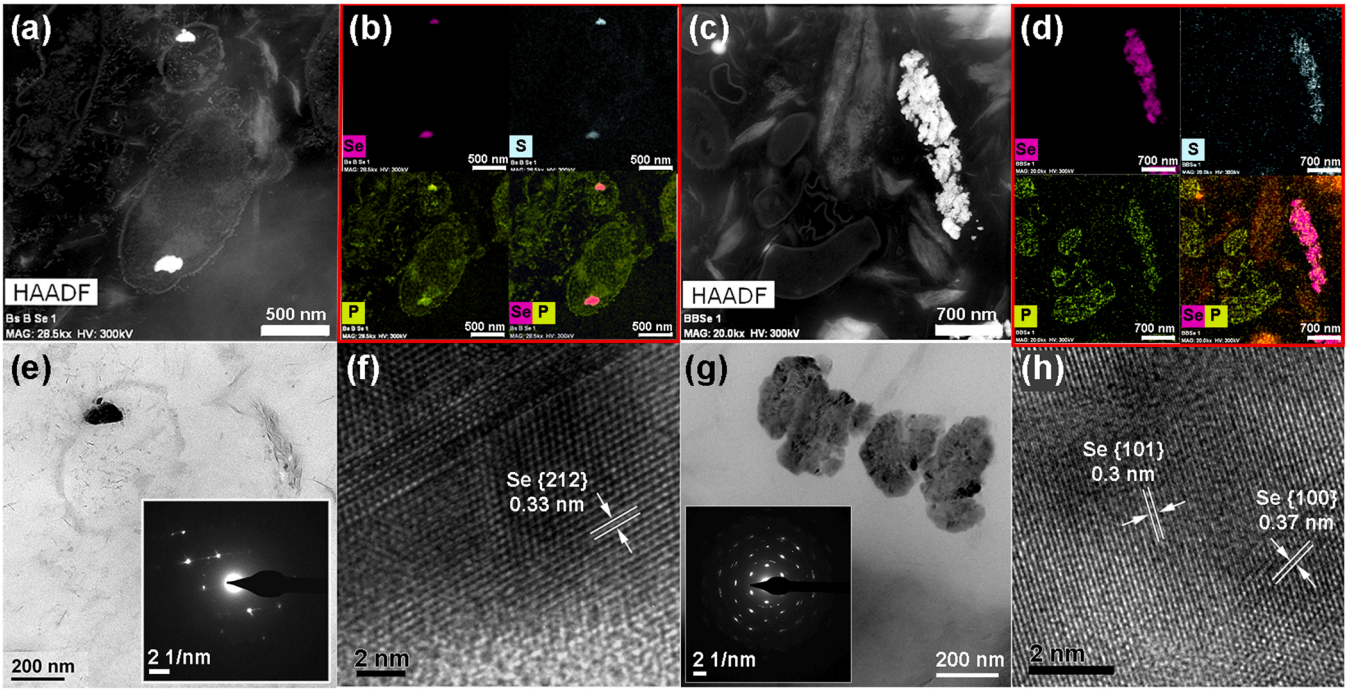

Fig. 3. High-Angle Annular Dark-Field Scanning Transmission Electron Microscopy (HAADF-STEM) imaging of SeNPs in the BsBSe (a), and BBSe (c) microcosms and their corresponding EDX maps with the elemental distribution of Se, S, and P, as well as combination of Se and P signals (b and d, respectively). High-Resolution Transmission Electron Microscopy (HRTEM) image of the SeNPs in the BsBSe (e) and BBSe (g) microcosms and their corresponding SAED patterns. HRTEM images of the intracellular *m*-SeNPs in BsBSe (f) and extracellular t-Se in BBSe (h) with lattice spacings.

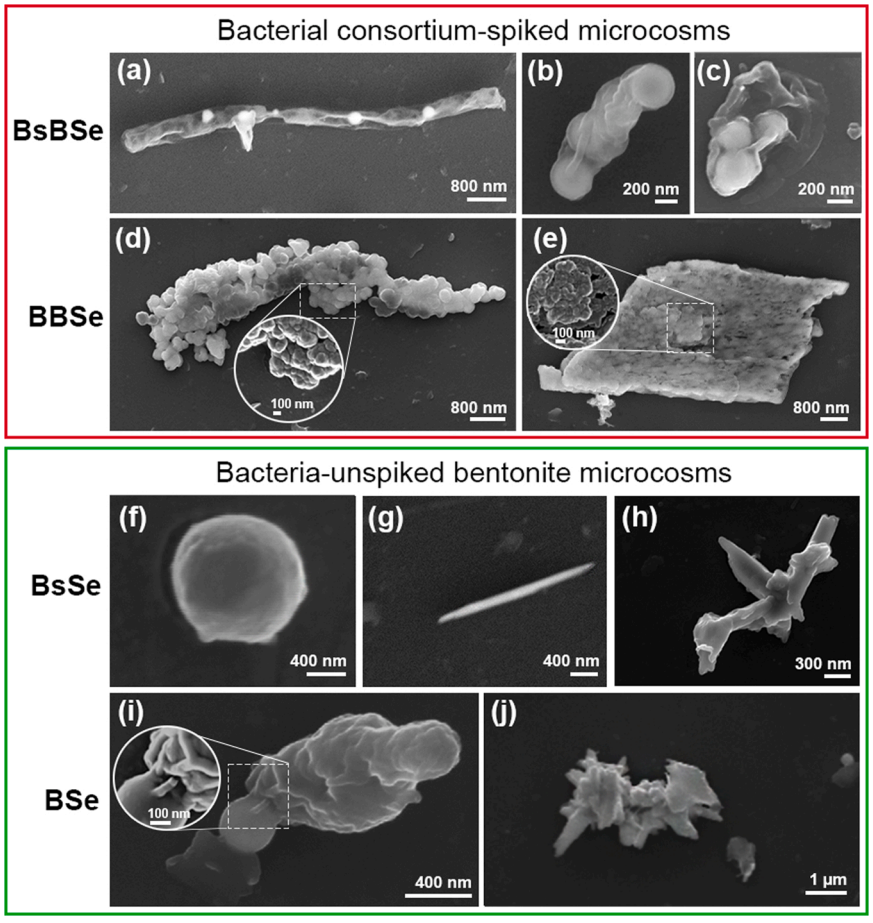

Fig. 4. Variable Pressure Field Emission Scanning Electron Microscopy (VP-FESEM) images of the SeNPs formed in BsBSe microcosms (a-c) corresponding to the SeNPs inside the bacterial cells (a) and associated to cell debris (b, and c); SeNPs formed in BBSe microcosms corresponding to growing Se crystals (d), and incipient crystal in form of aggregated SeNPs (e); SeNPs formed in BsSe microcosms corresponding to nanosphere (f), nanowire (g), and polygonal aggregates (h); SeNPs formed in BSe microcosms (i, and j). Images are shown in secondary electrons with the InLens detector performed at 5.00 kV (b, c, and h) and 10.0 kV (a, d, e, f, g, i, and j).

material (Fig. 4b, and c) as it was demonstrated by VP-FESEM. These SeNPs were probably formed inside the cells and then released to the extracellular space to be aggregated afterwards. Raman spectroscopy analyses were performed for these Se-nanospheres showing peaks at 251–252 cm^{-1}, which could be attributed to *a*-Se or crystalline *m*-Se (Fig. 5a).

In the case of BBSe sample, these electron-dense aggregates were found close to the bacterial cells (Fig. 3c). Element mapping analysis showed the presence of Se and S (Fig. 3d) with a SAED pattern indicating that these nanostructures were polycrystalline and indexed to *t*-Se (Fig. 3 g). The structure presented two distinct lattice spacings of 0.37 and 0.30 nm, corresponding to the (100) and (101) planes of *t*-Se, respectively (Fig. 3 h). These results are in accordance to VP-FESEM and Raman spectroscopy analyses (Figs. 4d, e, and 5a). Thus, Raman scattering spectrum derived from these Se nanostructures exhibited peaks at 235–236 cm^{-1} (Fig. 5a), attributed as well to *t*-Se (Lucovsky et al., 1967; Nagata et al., 1981). FESEM micrographs showed high number of big sized crystals of high dimensions that seemed to be formed by the aggregation of individual Se nanospheres (Fig. 4d, and e). All these Se-crystals were also composed of Se and S (Supplementary Fig. S3). These crystals were apparently growing both longitudinally and in height, as it was indicated by the edges and surface of the crystals (Fig. 4d and e).

3.3.2. *Unspiked natural/sterile and Se(IV)-amended bentonite (BSe and BsSe)*

Thin sections of the recovered orange layer of BsSe and BSe microcosms were studied by HAADF-STEM analysis and showed the presence of electron-dense nanostructures of different shapes and sizes (Fig. 6). Se crystalline nanostructures were observed in the BsSe microcosm (Fig. 6a, and e) as it was confirmed by EDX maps with the elemental composition and distribution showing signals of Se and S (Fig. 6b). Smectites were found surrounding SeNPs (Fig. 6a, and b). In the BSe sample, selenium was found in association to a large mineral phase identified as apatite (Fig. 6 c) as it was confirmed by EDX elemental mapping in Fig. 6d with Se, S, P and Ca signals.

In the BsSe sample, a monoclinic Se structure was also confirmed by HRTEM analyses, where the lattice spacing corresponding to 0.38 nm related to the (211) plane of *m*-Se was obtained (Fig. 6 f). This was also confirmed by Raman spectroscopy (Fig. 5b). At VP-FESEM, several sphere-shaped SeNPs (Fig. 4f), nanowires (Fig. 4g), and SeNPs aggregates (Fig. 4h) were observed. The Raman scattering spectrum derived from the individual Se nanospheres exhibited a peak at 252 cm^{-1} (Fig. 5b) which could be attributed to *a*-Se or *m*-Se (Lucovsky et al., 1967). The aggregated forms were apparently more crystalline than the individual nanospheres. A peak at 235 cm^{-1} corresponding to *t*-Se was observed for the Se polygonal aggregate and nanowires (Fig. 5b). This could indicate a transformation step from monoclinic to trigonal Se.

In the BSe sample, the SAED analyses indicated lattice spacings of 0.22 nm and 0.20 nm corresponding to the (111) plane of *t*-Se (Fig. 6g). HRTEM image of the nanowires showed a lattice spacing of 0.30 nm corresponding to the (101) plane of *t*-Se, (Fig. 6h). In Fig. 4i, the presence of Se nanospheres in BSe microcosms seemed to be released to the extracellular space because of cell lysis. Raman spectra derived from the SeNPs associated to debris revealed the presence of peaks at 254 cm^{-1} corresponding to *a*/*m*-Se. In addition, several SeNPs forming aggregates (Fig. 4j) presented a small peak at 236 cm^{-1} corresponding to symmetric stretching mode of *t*-Se (Fig. 5b).

3.4. *X-ray Absorption spectroscopy (XAS) analysis*

X-ray absorption spectroscopy (XAS) is an element specific synchrotron radiation-based technique able to provide detailed structural information concerning the oxidation state (X-ray absorption near-edge structure, XANES) and the structural parameters of the Se species and their allotropes distributed in the Se(IV) amended bentonites (Extended X-ray absorption fine structure, EXAFS).

The XANES region of the experimental (BBSe, BsBSe and BSe) and reference samples (representing different oxidation state of Se; Se(VI), Se(IV), and Se(0)), clearly showed that the local coordination of Se is dominated by Se^0 and none of the measured spectra are consistent with the Se(VI), Se(IV) standards (Fig. 7a, and Supplementary Fig. S4).

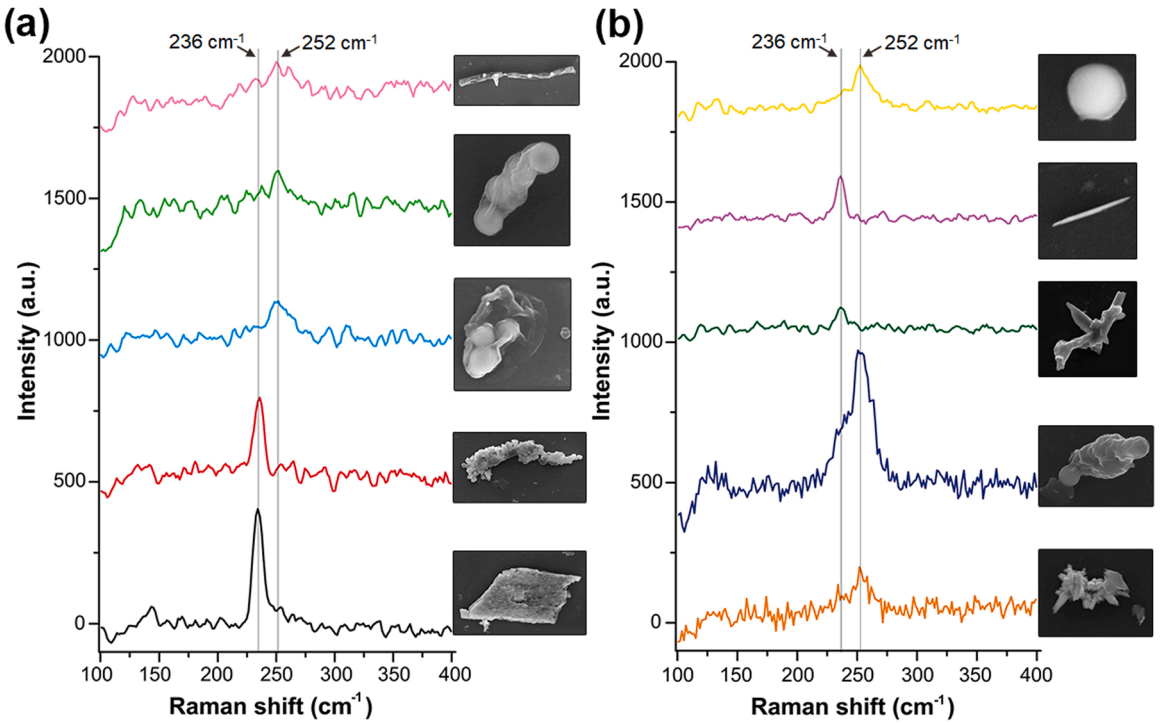

Fig. 5. Raman spectroscopy analyses derived from SeNPs in Fig. 4, corresponding with bacteria-spiked microcosms (a), and bacteria-unspiked microcosms (b). Spectra peaks are indicated by arrows: 236 cm^{-1} corresponded to *t*-Se and 252 cm^{-1} corresponded to *a*-/*m*-Se.

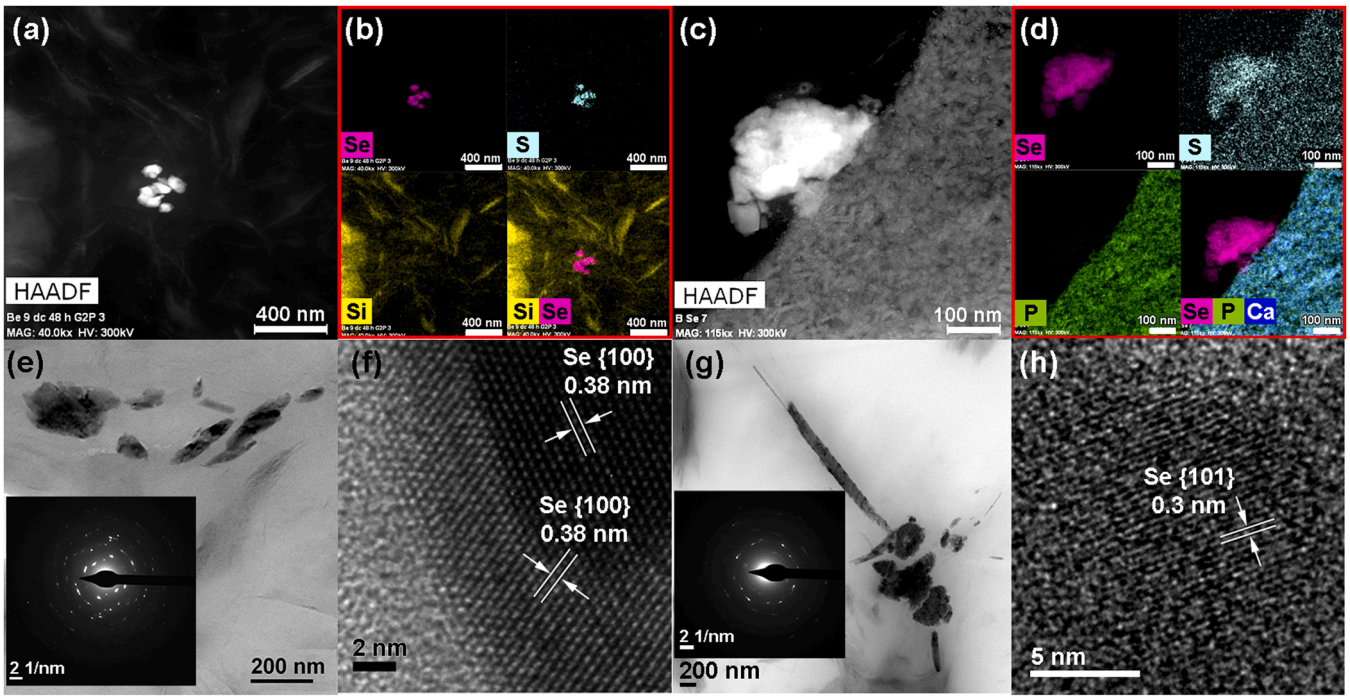

Fig. 6. High-Angle Annular Dark-Field Scanning Transmission Electron Microscopy (HAADF-STEM) imaging of SeNPs in the BsSe (a), and BSe (c) microcosms and their corresponding EDX maps. (b) The elemental distribution of Se, S, and Si, as well as combination of Se and Si signals in BsSe. (d) EDX maps of Se, S, P and combination of Se, P and Ca signals in BSe. High-Resolution Transmission Electron Microscopy (HRTEM) micrograph of the SeNPs in the BsSe (e) and BSe (g) microcosms and their corresponding SAED patterns. (f) HRTEM images of the intracellular *m*-SeNPs in BsSe and (h) extracellular *t*-Se in BSe, with their lattice spacing.

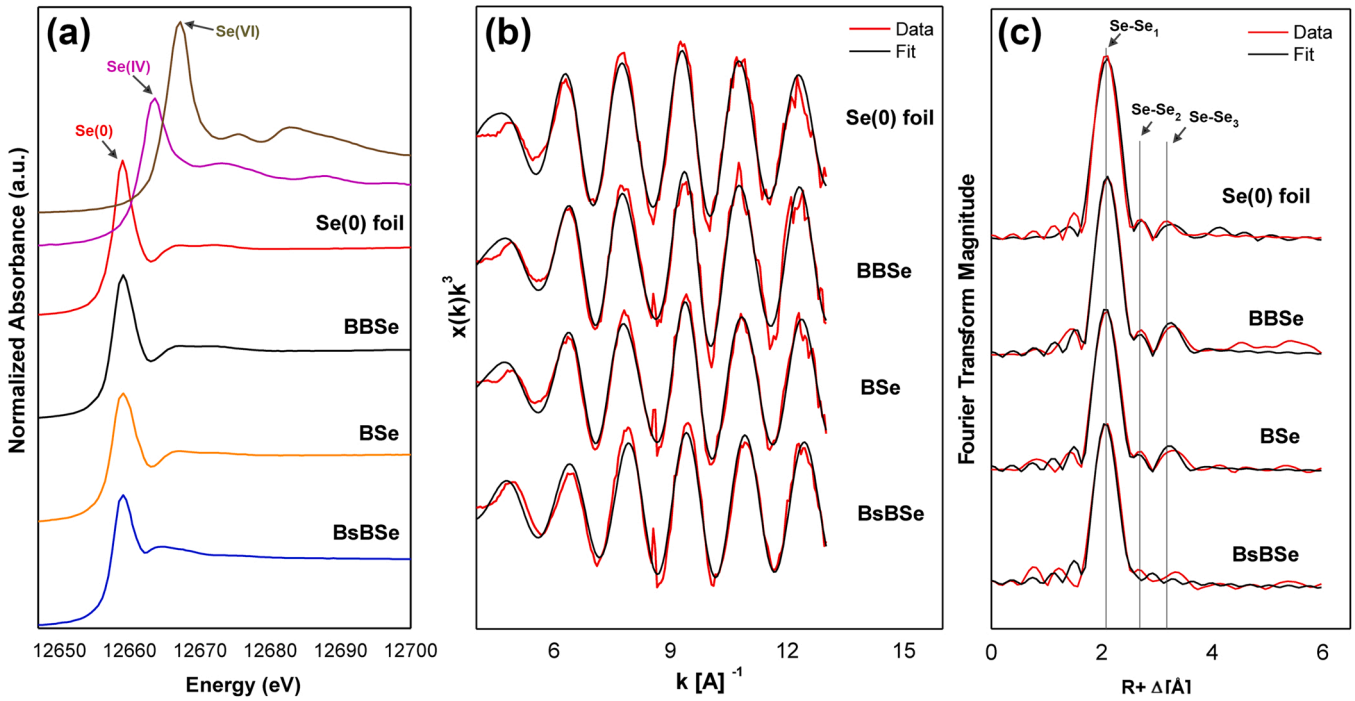

Fig. 7. XANES spectra of Se reference compounds [Se(IV)(Na_2SeO_3), Se(0)(Se foil) and Se(−II)(SeS_2)] and Se(IV)-amended bentonite microcosms for 6 months (a). EXAFS spectra of Se foil and bentonite samples (b) as well as their corresponding FT (c).

The EXAFS spectra of the Se-amended bentonite samples (BBSe, BsBSe and BSe) and Se foil (as Se^0 reference compound), along with their corresponding Fourier transforms (FT) and fit parameters of the calculated spectra, are respectively presented in Figs. 7b and 7c and Table 1. No good XAS signal of the sample BsSe was obtained due to low Se concentration in this sample.

FT peak distances are reported in units of Å and are expressed as R + ΔR. The fit of the EXAFS spectra of the three experimental samples indicated the presence of the first Se-Se_1 coordination shell at a bond distance of about 2.35–2.37 ± 0.002 Å (2.37 Å, 2.36 Å and 2.35 Å for

Table 1
EXAFS structural parameters of the Se foil and Se species formed in different Se (IV)- amended bentonite microcosms.

Sample	Shell	N[a]	R[Å][b]	σ^2 [Å^2][c]	ΔE[eV]
Se foil	Se-Se_1	3.4 ± 0.2	2.37	0.003	-6.2
	Se-Se_2	6.8[d]	3.31	0.018	
	Se-Se_3	3.4[d]	3.60	0.02	
BBSe	Se-Se_1	2.6 ± 0.1	2.37	0.003	-2.5
	Se-Se_2	5.2[d]	3.33	0.015	
	Se-Se_3	2.6[d]	3.64	0.010	
BSe	Se-Se_1	2.4 ± 0.1	2.36	0.003	-4.1
	Se-Se_2	4.8[d]	3.33	0.017	
	Se-Se_3	2.4[d]	3.64	0.010	
BsBSe	Se-Se_1	2.2 ± 0.1	2.35	0.0029	-2.6

[a] Errors in coordination numbers are ± 25% and standard deviations as estimated by EXAFSPAK;
[b] errors in distance are ± 0.02 Å;
[c] Debye-Waller factor
[d] Coordination number (N) linked to N of the shell Se-Se_1

the samples BBSe, BSe and BsBSe, respectively; Table 1). It is well known that the Se-Se_1 shell bond distance value depend upon the allotropic form of Se; 2.37 Å and 2.35 Å for trigonal and amorphous Se, respectively (Zhao et al., 2004; Breynaert et al., 2008). Accordingly, the main Se allotrope formed in the sample BBSe consisted with trigonal geometry as it was demonstrated by STEM/HAADF analysis (see Section 3.2.). This assumption is supported by the fact that the fit of EXAFS spectrum of this sample is improved (based on reduction of normalized fit error, data not shown) by the inclusion of the 2th and 3th Se-Se coordination shells at bond distance of 3.33 Å and 3.64 Å, respectively. These bond distances were similar to those of the trigonal Se(0) measured in this study as Se(0) foil and also slightly comparable to those associated with trigonal Se (3.39–3.43 Å for Se-Se_2 and 3.67–3.71 Å for Se-Se_2) reported by Ho et al. (2022). The Se-Se_1 bond distance of about 2.36 Å calculated for the sample BSe could correspond to an average distance value of 2.35 Å (amorphous Se) and 2.37 Å (trigonal Se). The presence of Se crystalline phase with a trigonal structure in this sample is also supported by the inclusion of the Se-Se_2 and Se-Se_3 coordination shells in the FT spectrum of this sample and by the results of STEM/HAADF (see below). In the case of the sample BsBSe, the main Se allotrope identified by EXAFS analysis correspond to amorphous Se (Se-Se_1 bond distance of about 2.35 Å) and no fit improvement was observed by the inclusion of Se-Se_2 and Se-Se_3 coordination shells in the FT spectrum.

3.5. Changes in microbial diversity of saturated-bentonite microcosms induced by sodium selenite

Total DNA of water-saturated bentonite microcosms was sequenced obtaining large diversity data of the microbial communities. Sterile bentonite samples (Bs) failed in the PCR amplification.

A total of 355 OTUs were classified at phylum (97.9%), class (92%), order (91.1%), family (87.1%) and genus (79.5%) levels. Richness (S), evenness and diversity of all the sequenced samples at each phylotype level were calculated using diversity indices (Shannon, Shannon's evenness, and Simpson) indicating a high bacterial diversity (ShannonD and SimpsonD) and a highly uniform distribution of OTUs (ShannonE) among the microcosms' microbial communities (Supplementary Fig. S5, Supplementary Table S2).

Sequences belonging to Archaea and Bacteria were identified. Although Bacteria were present in all the studied microcosms, the distribution of Archaea depended on the treatment, being almost or completely absent in Se(IV)-treated samples, with the exception of BBSe where they were represented by 21.9% of relative abundance (Supplementary Fig. S6).

Thirteen different bacterial phyla were annotated including statistically significant ones ($p < 0.005$) such as Firmicutes (33.1%), Proteobacteria (32.1%), Actinobacteria (13.5%), Bacteroidetes (0.3%), and Chloroflexi (0.15%), among others (Supplementary Fig. S6, Supplementary Tables S1-S4); in addition to the archaeal phylum Euryarchaeota (18.1%, $p = 0.000$). Interestingly, Euryarchaeota was significantly abundant ($p < 0.05$) in B, BB, and BBSe with 73.5%, 50.5%, and 21.5% of the total community, respectively. However, this archaeal phylum was almost or completely missing in BSe (0.2%), BsSe (0.1%) and BsBSe (0%), indicating a potential toxic effect of Se(IV).

Accentuated differences between microcosms were observed at genus level showing an effect of the tyndallization, the BSPAS consortium, and selenium amendment on the microbial community (Fig. 8, Supplementary Data S2 and S3). Firstly, as expected the heating treatment used to sterilize the bentonite influenced the microbial diversity. If statistically compared, the communities of BsSe and BSe showed *Symbiobacterium* (50.4%), *Paenibacillus* (2.6%) and *Bacillus* (1.7%), significantly more abundant ($p < 0.1$) in the "sterile" bentonite than in non-sterile ones (7.7, 0, 0%, respectively). However, *Desulfosporosinus* and the unclassified *Desulfuromonadaceae* were absent in BsSe but highly abundant in BSe, accounting for 22.4% and 10.1%, respectively ($p < 0.001$). Interestingly, *Anaerosolibacter* showed significantly ($p = 0.000$) higher relative abundance in BsBSe (28.7%) than in BBSe microcosms (1.3%) indicating a high survival to the heating treatment. In addition, *Pseudomonas*, included in the BSPAS consortium, accounted for 33.8% in BsBSe, and 2.5% in BBSe ($p = 0.000$). *Brachybacterium* was significantly ($p = 0.000$) dominant in the BsB microcosms in comparison with the BB samples, representing 89% of the community (Fig. 8, Supplementary Data S2 and S3).

The addition of BSPAS consortium affected the microbial diversity by shifting the indigenous bacterial community of the bentonite as it was observed in BBSe, BsBSe and BB, where members of this consortium were as expected more abundant in comparison with the unspiked samples (BSe, BsSe and B). Within the 50 genera analyzed by the ANOVA test ($p < 0.05$; $n = 3$), *Stenotrophomonas*, *Pseudomonas* and *Sedimentibacter* were significantly enriched in BBSe and BsBSe, in comparison with BSe and BsSe (Fig. 8, Supplementary Data S2 and S3). However, different genera significantly decreased their relative abundance ($p < 0.05$) in the spiked bentonite samples (BBSe, BsBSe and BB) in comparison with the controls (BSe, BsSe, and B, respectively) such as *Desulfosporosinus*, *Azotobacter*, *Actinotalea*, *Pseudomonas*, *Clostridium*, *Geobacter* and unclassified genera affiliated to *Desulfuromonadaceae*, *Propionibacteriaceae,* Clostridiales, and Methanomicrobiales, among others (Supplementary Data S3).

The impact of Se on the microbial community in the water-saturated bentonite microcosms was remarkable. The toxic effect of Se(IV) was mainly observed on the archaeal genus *Methanosarcina*, which was significantly abundant in BB (49.2%) and B (68.2%) ($p \leq 0.002$) in comparison with the Se-treated samples BBSe (21.5%) and BSe (0.2%) (Fig. 8, Supplementary Data S2 and S3). In view of these results, *Methanosarcina* could probably not tolerate the toxic effect of Se(IV) being unable to grow when soluble Se was present. However, in the BBSe sample it showed a significant abundance with respect to the rest of Se-treated samples. An explanation to this could be the removal of Se(IV) through its reduction to a less toxic Se(0) by biotic/abiotic processes. Other significant differences ($p < 0.05$) between Se-treated and untreated samples were related to *Stenotrophomonas* with 25.1% of total community in BBSe but only 1.44% in BB; *Desulfosporosinus* in BSe (22.4%) and BBSe (7.5%) in comparison with their controls B (6%) and BB (0.8%); *Anaerosolibacter* in BsBSe with 28.7% while in BsB it was represented by only 0.4% of relative abundance; and the unclassified genera affiliated to Firmicutes and *Desulfuromonadaceae* in BSe (13.2%, and 10.1%, respectively) with respect to B (1.3%, and 0%, respectively), among others.

If considering the microbial diversity distribution along the communities of the Se-treated and untreated microcosms, samples were grouped by PCoA analysis into different clusters, considering the relative abundance of the genera (Supplementary Fig. S7). In addition, the nine dominant genera in the samples and selenite were represented in a

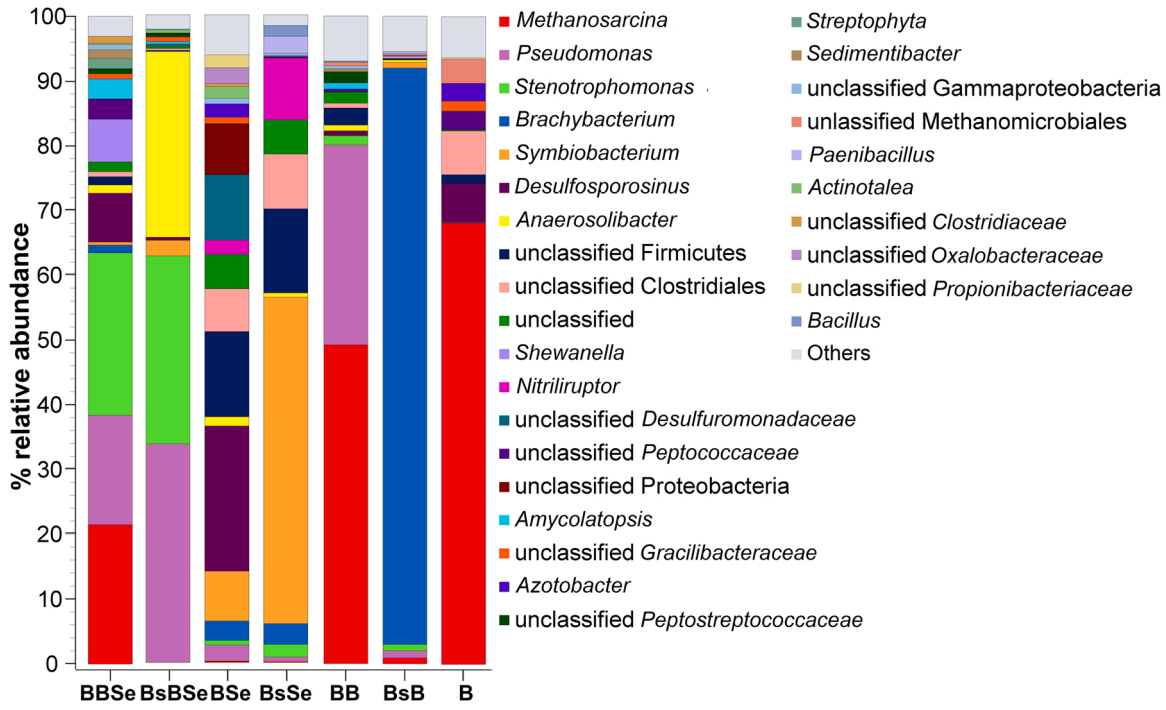

Fig. 8. Relative abundance of Bacteria and Archaea at genus level in all the water-saturated bentonite microcosms averaging triplicates (except for BB, BsB, and B, in duplicates) with a cut-off of 0.27% of the total community. B=bentonite, BB=bentonite spiked with BSPAS consortium, BsB= bentonite (sterile) spiked with BSPAS consortium, Se=sodium selenite treatment.

PCA plot (Fig. 9). The two main axes explained 60.9% of the total variation, of which 39% is explained by PC1, and 21.9% by PC2. As observed in the figure, BBSe and BB were clearly separated from the BSe and BsSe microcosms. Moreover, a clear effect of Se(IV) was observed in BsBSe samples, which were remarkably different from BsB (Fig. 9). The bacterial community in BsSe were positively correlated with higher Se (IV) final concentration, showing lower Se reduction rate. BsSe samples were characterized by higher relative abundance of *Symbiobacterium*. *Methanosarcina* was negatively correlated with selenite, being more representative of controls B and BB, and selenium-treated (BBSe) samples. In the case of BSe, the most representative bacterium was *Desulfosporosinus*, a sulfate-reducing bacterium potentially involved in selenium reduction. A heatmap was constructed to corroborate the differences between samples, showing that *Methanosarcina*, *Pseudomonas*, *Stenotrophomonas*, *Brachybacterium*, *Symbiobacterium*, *Desulfosporosinus* and unclassified genera affiliated to Firmicutes and Clostridiales were mainly involved in the samples' clustering (Supplementary Fig. S8).

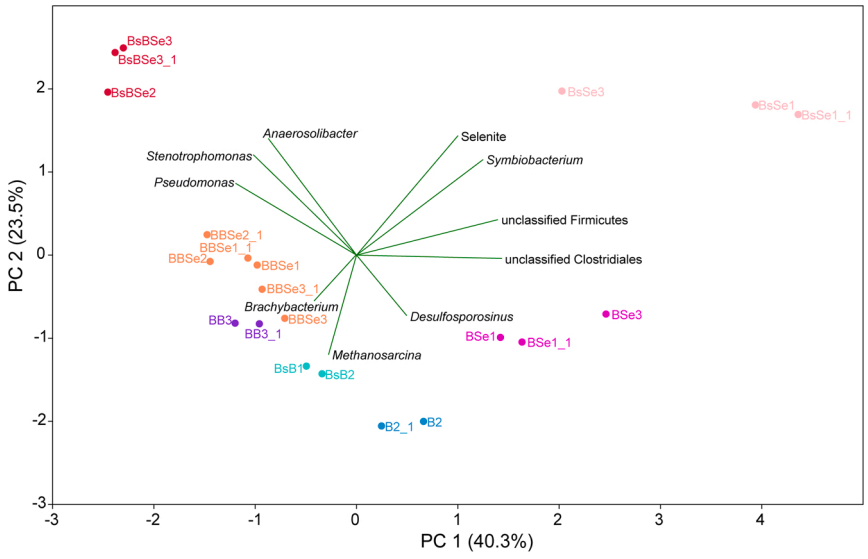

Fig. 9. Principal Components Analysis (PCA) plot comparing the microbial community structure considering the relative abundance of the nine dominant genera and selenite concentration after 6-month anaerobic incubation. Triplicates are represented (except for BBSe, BB, BsB, and B). B=bentonite, BB=bentonite spiked with BSPAS consortium, BsB=sterile bentonite (sterile) spiked with BSPAS consortium, Se=sodium selenite treatment.

4. Discussion

4.1. Effect of bentonite microbial communities on the chemical speciation of Se(IV)

4.1.1. Reduction of Se(IV) to Se(0) and the formation of SeNPs in the anaerobic water-saturated microcosms

Se-treated microcosms (BBSe, BsBSe, BSe and BsSe) changed their color, turning to orange and then to black throughout the incubation time. The orange color could correspond to amorphous Se nanospheres produced by the biotic reduction of Se(IV) into Se(0). Fernández-Llamosas et al. (2017) found amorphous Se nanospheres in a *Vibrio natriegens* pure culture, which turned orange/red after 12 and 24 h incubation in presence of 1 mM selenite. In addition, Tam et al. (2010) tested the capacity of *Shewanella* sp. HN-41 to reduce selenite producing amorphous Se(0) particles under anaerobic conditions. These shifts of colors are probably due to the reduction of Se(IV) and the formation of Se(0) nanostructures (Ruiz-Fresneda et al., 2018). A combination of state-of-the-art spectroscopic (EXAFS/XANES, Raman) and microscopic (STEM/HAADF, FESEM) techniques confirmed the presence of elemental selenium with different allotropic forms: amorphous, monoclinic and trigonal (see discussion below). In bentonites, selenite immobilization could be mediated by abiotic and/or biotic processes (Wang et al., 2022). Several works reported that abiotic retention of Se (IV) in the bentonite would happen through processes such as: i) adsorption to the bentonite mineral surfaces, or ii) reduction to Se(0) by pyrite (FeS_2), siderite minerals, and even by the structural Fe(II) in smectites (Breynaert et al., 2010; Hoving et al., 2019; Kang et al., 2011). Adsorption method has been described as an effective way of removing heavy metal cations and metalloid anions especially successful for selenium, which is usually linked to pyrite or other adsorbents such as clay, aluminium oxides, and ferric oxyhydroxides (He et al., 2018). Accordingly, in this study, microscopic and associated EDX analyses of the BSe microcosms showed peaks of Se associated to smectite. This was probably achieved by the Se(IV) adsorption to the surface of this mineral phase (Urík et al., 2018; Xu et al., 2021). This finding was in line with the study of Hoving et al. (2019), reporting that pyrite could be the most relevant reductant of selenite, which is reduced to Se(0) as a result of an electron transfer from this mineral clay to the metalloid. However, in the Spanish bentonite, the pyrite content is very low ($0.02 \pm 0.01\%$) (Fernández et al., 2000). Therefore, the reduction of Se(IV) to Se(0) occurred in these samples could not be attributed to pyrite. In addition, a big-sized apatite was found to be associated to SeNPs in the BSe sample. This apatite could be formed by the activity of bentonite indigenous microorganisms enriched by the addition of G2P. Some of the bentonite native bacteria such as *Stenotrophomonas*, *Symbiobacterium* and *Brachybacterium* have been described for their phosphatase activity releasing inorganic phosphate ($_{Pi}$) from the organic phosphate source (G2P) (Hoang et al., 2014; Sánchez-Castro et al., 2017; Shiratori-Takano et al., 2014). This $_{Pi}$ could react with the Ca originated from the dissolution of calcite to induce the precipitation of apatite. Duc et al. (2003) showed the sorption of selenite groups on the apatite surface. The sorbed selenium was embedded in the crystallographic sites where phosphorus is normally located, indicating that the Se sorption process on the apatite is commonly mediated by an anionic exchange with phosphate groups.

Biotic processes seem to be the most probable mechanisms involved in the reduction of Se(IV) and formation of Se(0) nanostructures in the studied bentonite microcosms. A high number of works have described the reduction of Se(IV) to Se(0) by pure cultures of bacterial strains such as the Spanish bentonite isolate *S. bentonitica* (Ruiz-Fresneda et al., 2019, 2018, 2020), *Pseudomonas seleniipraecipitans* (Hunter, 2014), *P. putida* (Avendaño et al., 2016), *P. aeruginosa* (Dwivedi et al., 2013), *Shewanella oneidensis* (Li et al., 2014) and *Pediococcus acidilactici* (Kousha et al., 2017), among others. Javed et al. (2015) investigated the selenite reduction by numerous bacterial strains (*Bacillus subtilis*, *B. licheniformis*, *Exiguobacterium* sp., and *P. pseudoalcaligenes*) isolated from polluted environments. However, to the best of our knowledge, this is the first work describing the reduction of Se(IV) within a ternary system containing three components: microbes, bentonite, and Se. In this system, bentonite plays a key role since it could contribute to selenium reduction through abiotic (pyrite, siderite minerals, and Fe(II) of smectites) and biotic (bacterial community) processes. Whilst in pure cultures (a system with only bacteria and Se), the Se reduction is mediated by one known bacterium in very controlled conditions (culture media, homogenous Se concentration, uniform temperature, etc.). In our experiment, the reduction of Se(IV) to Se(0) and the subsequent formation of SeNPs could be driven by the activity of the bentonite indigenous bacteria and/or the bacterial strains of the inoculated BSPAS consortium. Several Se nanostructures different in size, morphology, crystallinity and localization were detected using state-of-the-art microscopic and spectroscopic techniques. Regarding the localization, the intracellular and debris-associated SeNPs presented a spherical morphology while extracellular Se nanostructures were mainly hexagonal or forming crystalline aggregates. Interestingly, the intracellular Se nanospheres seemed to be expelled out from the cells in BSe samples, appearing inside the cells probably linked to the plasmatic membrane or associated to cell debris in the BsBSe microcosms. Different mechanisms have been proposed to highlight the process by which the Se is reduced inside the bacterial cell (Hunter et al., 2014, Li et al., 2014; Pinel-Cabello et al., 2021; Ruiz-Fresneda et al., 2018). An explanation to this process could be that the intracellular reduction of Se(IV) is mediated by molecules containing reduced thiols groups (-SH) such as glutathione (GSH). Selenite reacts with GSH producing selenodiglutathione (GS-Se-SG), which is then reduced to selenopersulfide ($GS\text{-}Se^-$) by NADPH in presence of glutathione reductase (GS). The unstable selenopersulfide finally dismutates into GSH and Se(0) (Li et al., 2014; Ruiz-Fresneda et al., 2018). Hunter (2014) detected genes for GS and for the thioredoxin reductase (similar to GS) in *P. seleniipraecipitans*. In addition, Pinel-Cabello et al. (2021) found an increase in the presence of several proteins potentially involved in Se(IV) reduction (glutathione reductase, glutathione-disulfide reductase and thioredoxin-disulfide reductase) in *S. bentonitica* BII-R7 culture treated with Se(IV). Other mechanisms are based on the activity of reductases that directly reduce Se(IV) to Se(0) such as nitrite reductase in *Rhizobium sullae* (Basaglia et al., 2007), fumarate reductase in *S. oneidensis* (Li et al., 2014), and selenite reductase in *Bacillus selenitireducens* (Wells et al., 2019). Sarret et al. (2005) reported that the Se(IV) reduction resulted into intracellular granules of monoclinic Se(0) in the cells of *Ralstonia metallidurans*. Furthermore, Li et al. (2014) found that the fumarate reductase could catalyze the reduction of Se(IV) to Se(0) in the periplasmic space, acquiring the required electrons from the *c*-type cytochrome.

4.1.2. Biotransformation of amorphous Se nanospheres to trigonal Se

Selenium can exist in three different allotropes: amorphous (red *a*-Se), monoclinic (*m*-Se) and trigonal (grey/black *t*-Se). The *a*-Se is thermodynamically unstable and undergoes transformation to *m*-Se at high temperatures. In addition, *m*-Se is metastable and could also eventually suffer conversion to the *t*-Se (Goldan et al., 2016). Moreover, pure culture of several bacterial strains like those present in the amended microcosms or enriched in unspiked samples (e.g. *S. bentonitica* BII-R7; *Pseudomonas* sp., *Bacillus* sp.) are able to transform *a*-Se nanospheres to the more stable *t*-Se nanostructures (Bueno-Galera, 2019; Ruiz-Fresneda et al., 2020, 2019, 2018). In the present work, the different allotropic forms of elemental Se (amorphous, monoclinic and trigonal) were observed in all the Se-treated samples (BBSe, BsBSe, BSe, and BsSe) using SAED, HRTEM, Raman spectroscopy, and EXAFS analyses. The extracellular and intracellular Se nanospheres turned to be monoclinic phases of crystalline Se in the BSe, BsSe, and BsBSe samples. The transformation of *m*-Se into *t*-Se could be observed in BBSe at macroscopic level by the shift in the color of the layer deposited on the top of the bentonite: an orange layer was detected in the first 30 days of the anaerobic incubation, but with the time it was gradually turning to

dark grey/black layer corresponding to *t*-Se. This change in color was described by Wang et al. (2010) in a *B. subtilis* culture after 24 h of incubation, being the orange color at time 0 corresponding to colloids of nanospheres of *a*-Se/*m*-Se, but after 12 h a mixture of these *m*-Se and nanowires of *t*-Se were obtained.

Several hypotheses were described to explain the transformation of amorphous to monoclinic and then to stable trigonal Se phases. Thus, the unstable *m*-Se could be dissolved and the released Se would be deposited on the *t*-Se nanocrystals acting as precursors and allowing the uniform growth of nanowires, hexagonal or larger-sized crystals of *t*-Se (Wang et al., 2010). In contrast to what happens in *m*-Se with weak van der Waals forces between the eight-atom units, the *t*-Se consists of polymeric helical chains of Se atoms parallel to each other and where every individual atom is connected with partial metallic bonds to four nearby Se atoms in the adjacent chains conferring, thus, high stability to the whole molecule (Fernández-Martínez and Charlet, 2009; Goldan et al., 2016). Accordingly, Ruiz-Fresneda et al. (2018) hypothesized an analogous process occurring in *S. bentonitica* pure culture, isolated from Spanish bentonites, consistent with our experimental findings. They reported intracellular Se nanospheres in *S. bentonitica* cells, which were released out of the cells after 48 h of incubation, and finally they aggregate in the extracellular space and transform to *t*-Se after 144 h of incubation.

EXAFS analysis confirmed that the Se allotropic biotransformation showed a Se crystallization process in the studied bentonite microcosms (transformation from *a*-Se to *t*-Se) was observed in the samples. Accordingly, a Se crystallization process decrease according to the following order: BBSe, BSe, and BsBSe.

4.2. Impact of selenite on the microbial diversity of water-saturated bentonite

The microbial community in the bentonite could be influenced by different physico-chemical factors (*e.g.*, pH, electron donors). For instance, the addition of acetate in our experiment enriched the archaea *Methanosarcina*, which is the only genus (beside *Methanothrix*) with the capacity to grow using acetate for the methanogenic activity (aceticlastic pathway) to produce CH_4 and CO_2 (Ferry, 2020). However, the present work indicated that Se(IV) negatively affected the distribution of autochthonous bacterial and archaeal communities in the bentonites. *Methanosarcina* was unable to grow in presence of Se(IV) showing low relative abundance in almost all selenite-treated microcosms (BsBSe, BSe and BsSe). Although, in the case of bentonite microcosms inoculated with BSPAS consortium (BBSe), *Methanosarcina* seemed to regain its ability to grow occurring with a relative abundance of 21.5%. The tolerance of this microorganism to Se could be enhanced by the total reduction of Se(IV) to Se(0) by members of the inoculated consortium, which decrease the rate of soluble and available Se in the system (Avendaño et al., 2016; Hunter, 2014; Ruiz-Fresneda et al., 2019, 2018). On the other hand, *Amycolatopsis* was found to be enriched in high-Se soils where this metalloid was present as a mixture of Se(IV) and Se (VI) at an average concentration of $>$ 30 mg/kg (Rosenfeld et al., 2018).

The presence of Se(IV) enhanced the occurrence of bacteria with Se-detoxification mechanisms such as *Pseudomonas* and *Stenotrophomonas*. Several sequences belonging to these bacteria were found in the samples where BSPAS were not spiked (BSe and BsSe) indicating that they were naturally occurring in the studied bentonites and enriched by the addition of sodium acetate in the microcosms. The growth of these bacteria is actually stimulated by using this organic acid as electron and carbon sources (Gonzalez-Gil et al., 2016; Sánchez-Castro et al., 2017; Yang et al., 2019). In addition, indigenous bacteria such as *Desulfosporosinus* and unclassified *Desulfuromonadaceae* were found to be highly abundant in BSe microcosms in comparison to the untreated samples (B) indicating their tolerance to the toxic selenite. Belonging to the group of sulfate-reducing bacteria (SRB), these microorganisms have been previously described for their capacity to couple the oxidation of lactate or acetate to Se oxyanion reduction to Se(0) (Hockin and Gadd, 2006, 2003; Nancharaiah and Lens, 2015). Hockin and Gadd (2003) reported a coprecipitation of Se(0) and S in the extracellular space, as a result of a dissimilatory sulfate reduction producing sulfide and a subsequent exothermic oxidation-reduction reaction involving this sulfide and selenite. This produces spherical nanoparticles that were associated to the cell surfaces (outside cell walls).

Interestingly, unclassified genera affiliated to Firmicutes and Clostridiales were detected with high relative abundance in BSe and BsSe indicating a high resistance to the heat pressure and tolerance to selenite. In line with this finding, Povedano-Priego et al. (2022) identified members of Clostridia in anaerobic microcosms treated with glycerol-2-phosphate revealing their ability to use this substrate as energy source. Their presence in the BsSe could demonstrate their capacity to resist adverse conditions (e.g., heating) by the production of endospores, which can germinate afterwards when favorable conditions reach the ecosystem (Xiao et al., 2011). For instance, the availability of glycerol promoted the growth of *Clostridium* and other members of Clostridia in bentonite samples (Biebl, 2001; Patil et al., 2016). Clostridia in selenite-treated microcosms could play an important role in the selenium immobilization. Gonzalez-Gil et al. (2016) also found that the abundance of Clostridia increased after 21 days of exposure to selenite in anaerobic sludge. In addition, several studies described the capacity of *Clostridium* to precipitate Se as Se(0) through an enzymatically active process (Bao et al., 2013; Gonzalez-Gil et al., 2016).

5. Conclusions

Based on all the above observations, we suggest that similarly to the previously described in the bacterial pure cultures, a Se(IV) biotransformation process also occurs in the complex ternary microbes/bentonite/Se microcosms. Firstly, a reduction of selenite into elemental selenium is mediated by the activity of potential periplasmic-reductase enzymes resulting in the accumulation of Se(0) in the periplasmic space. Secondly, the red-orange *a*-Se and *m*-Se nanoparticles are released to and aggregated in the extracellular environment. Finally, the unstable nature of the *m*-Se particles further leads to its solubilization and re-crystallization into the more stable form of *t*-Se, producing thus the growth of nanowires and large-polygonal crystals of Se(0). The formation of less soluble *t*-Se nanostructures significantly contributes to the hindering of the selenium mobility in the environment. The presence of Se(IV) impacts the microbial diversity of bentonite microcosms, negatively when the microbial growth (e.g. *Methanosarcina*) is inhibited by the toxic effect of Se(IV), and positively when Se(IV)-tolerant bacteria (e.g. *Pseudomonas*, *Stenotrophomonas*, *Desulfosporosinus*) are enriched for their potential capacity to reduce selenite. This work is thus relevant for understanding the biogeochemical processes, occurring at the interface bentonite/microbes, and their impacts on the chemical speciation of Se, providing novel insights into the deep geological disposal of radioactive waste. Further study is required however to disentangle the processes that may occur in the system in the long term.

Funding

This work was supported by the project RTI2018.101548.B.I00 to M. L.M and the grant FPU 14/04263 to the first author from the "Ministerio de Educación Cultura y Deporte" (Spanish Government).

CRediT authorship contribution statement

Cristina Povedano-Priego: Conceptualization, Methodology, Validation, Investigation, Formal analysis, Visualization, Writing – original draft, Writing – review & editing. **Fadwa Jroundi**: Methodology, Validation, Investigation, Supervision, Writing – review & editing. **Pier L. Solari**: Methodology, Formal Analysis, Writing – review & editing. **Isabel Guerra-Tschuschke**: Resources, Investigation. **Maria del Mar**

Abad-Ortega: Resources, Investigation. **Alexander Link**: Resources, Investigation. **Ramiro Vilchez-Vargas**: Validation, Formal analysis, Investigation, Writing – review & editing. **Mohamed L. Merroun**: Conceptualization, Methodology, Formal analysis, Resources, Writing – original draft, Writing – review & editing, Supervision, Project administration, Funding acquisition.

Environmental Implication

Bentonites constitute the artificial barrier in the future Deep Geological Repositories (DGR) of hazardous radioactive waste (e.g. ^{79}Se isotope as fission product). The present study reported for the first time the impact of bentonite microbial populations on the mobility of selenium(IV), simulating the worst scenario of radionuclide accidental leakage from nuclear waste repository. Enrichment of bacterial groups involved in reduction of Se(IV) to Se(0) and allotropic biotransformation of amorphous to trigonal Se(0) nanorods with high settleability was demonstrated. The formation of trigonal Se(0) could have positive environmental implications in the safety of future DGR and in the bioremediation of hazardous Se.

Declaration of Competing Interest

The authors declare that they have no known competing financial interests or personal relationships that could have appeared to influence the work reported in this paper.

Data availability

Sequencing data are available in NCBI platform with the accession number PRJNA877829.

Acknowledgments

This work was supported by grant RTI2018.101548.B.I00 to M.L.M. We acknowledge the assistance of Concepción Hernández-Castillo for the preparation of samples for microscopic analyses, and members of Centro de Instrumentación Científica (University of Granada, Spain). AL and RVV are supported by the funds of European Commission through the "European funds for regional development" (EFRE) as well as by the regional Ministry of Economy, Science and Digitalization of Saxony-Anhalt as part of the "Autonomy in old Age" (AiA) research group for "LiLife" Project (Project ID: ZS/2018/11/95324). Funding for open access charge: Universidad de Granada / CBUA.

Appendix A. Supporting information

Supplementary data associated with this article can be found in the online version at doi:10.1016/j.jhazmat.2022.130557.

References

Anderson, C., Johnsson, A., Moll, H., Pedersen, K., 2011. Radionuclide geomicrobiology of the deep biosphere. Geomicrobiol. J. 28, 540–561. https://doi.org/10.1080/01490451.2010.507644.

Ankudinov, A.L., Ravel, B., Rehr, J.J., Conradson, S.D., 1998. Real-space multiple-scattering calculation and interpretation of x-ray-absorption near-edge structure. Phys. Rev. B 58, 7565–7576. https://doi.org/10.1103/PhysRevB.58.7565.

Ansede, J.H., Yoch, D.C., 1997. Comparison of selenium and sulfur volatilization by dimethylsulfoniopropionate lyase (DMSP) in two marine bacteria and estuarine sediments. FEMS Microbiol Ecol. 23, 315–324. https://doi.org/10.1111/j.1574-6941.1997.tb00412.x.

Avendaño, R., Chaves, N., Fuentes, P., Sánchez, E., Jiménez, J.I., Chavarría, M., 2016. Production of selenium nanoparticles in *Pseudomonas putida* KT2440. Sci. Rep. 6, 1–9. https://doi.org/10.1038/srep37155.

Bao, P., Huang, H., Hu, Z.-Y., Häggblom, M.M., Zhu, Y.-G., 2013. Impact of temperature, CO_2 fixation and nitrate reduction on selenium reduction, by a paddy soil *Clostridium* strain. J. Appl. Microbiol. 114, 703–712. https://doi.org/10.1111/jam.12084.

Basaglia, M., Toffanin, A., Baldan, E., Bottegal, M., Shapleigh, J.P., Casella, S., 2007. Selenite-reducing capacity of the copper-containing nitrite reductase of *Rhizobium sullae*. FEMS Microbiol Lett. 269, 124–130. https://doi.org/10.1111/j.1574-6968.2006.00617.x.

Beaver, R.C., Engel, K., Binns, W.J., Neufeld, J.D., 2022. Microbiology of barrier component analogues of a deep geological repository. Can. J. Microbiol. 68, 73–90. https://doi.org/10.1139/cjm-2021-0225.

Bengtsson, A., Pedersen, K., 2017. Microbial sulphide-producing activity in water saturated Wyoming MX-80, Asha and Calcigel bentonites at wet densities from 1500 to 2000kgm^{-3}. Appl. Clay Sci. 137, 203–212. https://doi.org/10.1016/j.clay.2016.12.024.

Biebl, H., 2001. Fermentation of glycerol by *Clostridium pasteurianum*–batch and continuous culture studies. J. Ind. Microbiol. Biotechnol. 27, 18–26. https://doi.org/10.1038/sj/jim/7000155.

Bohorquez, L.C., Delgado-Serrano, L., López, G., Osorio-Forero, C., Klepac-Ceraj, V., Kolter, R., Junca, H., Baena, S., Zambrano, M.M., 2012. In-depth Characterization via Complementing Culture-Independent Approaches of the Microbial Community in an Acidic Hot Spring of the Colombian Andes. Micro Ecol. 63, 103–115. https://doi.org/10.1007/s00248-011-9943-3.

Breynaert, E., Bruggeman, C., Maes, A., 2008. XANES-EXAFS analysis of se solid-phase reaction products formed upon contacting Se(IV) with FeS_2 and FeS. Environ. Sci. Technol. 42, 3595–3601. https://doi.org/10.1021/es071370r.

Breynaert, E., Scheinost, A.C., Dom, D., Rossberg, A., Vancluysen, J., Gobechiya, E., Kirschhock, C.E.A., Maes, A., 2010. Reduction of Se(IV) in boom clay: XAS solid phase speciation. Environ. Sci. Technol. 44, 6649–6655. https://doi.org/10.1021/es100569e.

Bueno-Galera, C., 2019. Caracterización espectroscópica y microscópica de la biosíntesis microbiana de SeNPs y el papel de las proteínas en su formación. Universidad de Granada,.

Chen, H., Shin, D.-W., Nam, J.-G., Kwon, K.-W., Yoo, J.-B., 2010. Selenium nanowires and nanotubes synthesized via a facile template-free solution method. Mater. Res. Bull. 45, 699–704. https://doi.org/10.1016/j.materresbull.2010.02.016.

Duc, M., Lefevre, G., Fedoroff, M., Jeanjean, J., Rouchaud, J.C., Monteil-Rivera, F., Dumonceau, J., Milonjic, S., 2003. Sorption of selenium anionic species on apatites and iron oxides from aqueous solutions. J. Environ. Radioact., Int. Workshop Mobil. Iodine, technetium, Selenium Uranium biosphere 70, 61–72. https://doi.org/10.1016/S0265-931X(03)00125-5.

Dwivedi, S., AlKhedhairy, A.A., Ahamed, M., Musarrat, J., 2013. Biomimetic synthesis of selenium nanospheres by bacterial strain JS-11 and its role as a biosensor for nanotoxicity assessment: a novel Se-bioassay. PLOS ONE 8, e57404. https://doi.org/10.1371/journal.pone.0057404.

Eswayah, A.S., Smith, T.J., Gardiner, P.H.E., 2016. Microbial transformations of selenium species of relevance to bioremediation. Appl. Environ. Microbiol 82, 4848–4859. https://doi.org/10.1128/AEM.00877-16.

Fernández, A.M., Cuevas, J., Rivas, P., 2000. Pore water chemistry of the febex bentonite. MRS Online Proc. Libr. 663, 573. https://doi.org/10.1557/PROC-663-573.

Fernández-Llamosas, H., Castro, L., Blázquez, M.L., Díaz, E., Carmona, M., 2017. Speeding up bioproduction of selenium nanoparticles by using *Vibrio natriegens* as microbial factory. Sci. Rep. 7, 1–9. https://doi.org/10.1038/s41598-017-16252-1.

Fernández-Martínez, A., Charlet, L., 2009. Selenium environmental cycling and bioavailability: a structural chemist point of view. Rev. Environ. Sci. Biotechnol. 8, 81–110. https://doi.org/10.1007/s11157-009-9145-3.

Ferry, J.G., 2020. Methanosarcina acetivorans: a model for mechanistic understanding of aceticlastic and reverse methanogenesis. Front. Microbiol 0. https://doi.org/10.3389/fmicb.2020.01806.

Garbisu, C., Ishii, T., Leighton, T., Buchanan, B.B., 1996, Bacterial reduction of selenite to elemental selenium. Chemical Geology, Chemical And Biological Control On Mineral Growth And Dissolution Kinetics, American Chemical Society Meeting 132, 199–204. https://doi.org/10.1016/S0009–2541(96)00056–3.

Goldan, A.H., Li, C., Pennycook, S.J., Schneider, J., Blom, A., Zhao, W., 2016. Molecular structure of vapor-deposited amorphous selenium. J. Appl. Phys. 120, 135101 https://doi.org/10.1063/1.4962315.

Gonzalez-Gil, G., Lens, P.N.L., Saikaly, P.E., 2016. Selenite reduction by anaerobic microbial aggregates: microbial community structure, and proteins associated to the produced selenium spheres. Front. Microbiol 7. https://doi.org/10.3389/fmicb.2016.00571.

Grigoryan, A.A., Jalique, D.R., Medihala, P., Stroes-Gascoyne, S., Wolfaardt, G.M., McKelvie, J., Korber, D.R., 2018. Bacterial diversity and production of sulfide in microcosms containing uncompacted bentonites. Heliyon 4. https://doi.org/10.1016/j.heliyon.2018.e00722.

Guerra, I., Cardell, C., 2015. Optimizing use of the structural chemical analyser (variable pressure FESEM-EDX Raman spectroscopy) on micro-size complex historical paintings characterization. J. Microsc. 260, 47–61. https://doi.org/10.1111/jmi.12265.

Han, D.S., Batchelor, B., Abdel-Wahab, A., 2012. Sorption of selenium(IV) and selenium (VI) onto synthetic pyrite (FeS2): Spectroscopic and microscopic analyses. J. Colloid Interface Sci. 368, 496–504. https://doi.org/10.1016/j.jcis.2011.10.065.

He, Y., Xiang, Y., Zhou, Y., Yang, Y., Zhang, J., Huang, H., Shang, C., Luo, L., Gao, J., Tang, L., 2018. Selenium contamination, consequences and remediation techniques in water and soils: A review. Environ. Res. 164, 288–301. https://doi.org/10.1016/j.envres.2018.02.037.

Ho, M.S., Vettese, G.F., Morris, K., Lloyd, J.R., Boothman, C., Bower, W.R., Shaw, S., Law, G.T.W., 2022. Retention of immobile Se(0) in flow-through aquifer column systems during bioreduction and oxic-remobilization. Sci. Total Environ. *834*. https://doi.org/10.1016/j.scitotenv.2022.155332.

Hoang, V.-A., Kim, Y.-J., Nguyen, N.-L., Yang, D.-C., 2014. *Brachybacterium ginsengisoli* sp. nov., isolated from soil of a ginseng field. Int. J. Syst. Evol. Microbiol 64, 3063–3068. https://doi.org/10.1099/ijs.0.058388-0.

Hockin, S., Gadd, G.M., 2006. Removal of selenate from sulfate-containing media by sulfate-reducing bacterial biofilms. Environ. Microbiol. 8, 816–826. https://doi.org/10.1111/j.1462-2920.2005.00967.x.

Hockin, S.L., Gadd, G.M., 2003. Linked Redox Precipitation of Sulfur and Selenium under Anaerobic Conditions by Sulfate-Reducing Bacterial Biofilms. Appl. Environ. Microbiol 69, 7063–7072. https://doi.org/10.1128/AEM.69.12.7063-7072.2003.

Hoving, A.L., Münch, M.A., Bruggeman, C., Banerjee, D., Behrends, T., 2019. Kinetics of selenite interactions with Boom Clay: adsorption–reduction interplay. Geol. Soc., Lond., Spec. Publ. 482, 225–239. https://doi.org/10.1144/SP482-2018-60.

Hunter, W.J., 2014. *Pseudomonas seleniipraecipitans* Proteins Potentially Involved in Selenite Reduction. Curr. Microbiol 69, 69–74. https://doi.org/10.1007/s00284-014-0555-2.

Javed, S., Sarwar, A., Tassawar, M., Faisal, M., 2015. Conversion of selenite to elemental selenium by indigenous bacteria isolated from polluted areas. Chem. Speciat. Bioavailab. 27, 162–168. https://doi.org/10.1080/09542299.2015.1112751.

Jörg, G., Bühnemann, R., Hollas, S., Kivel, N., Kossert, K., Van Winckel, S., Gostomski, C. L., 2010. Preparation of radiochemically pure ^{79}Se and highly precise determination of its half-life. Appl. Radiat. Isot. v (68), 2339–2351. https://doi.org/10.1016/j.apradiso.2010.05.006.

Kang, M., Chen, F., Wu, S., Yang, Y., Bruggeman, C., Charlet, L., 2011. Effect of pH on Aqueous Se(IV) Reduction by Pyrite. Environ. Sci. Technol. 45, 2704–2710. https://doi.org/10.1021/es1033553.

Kousha, M., Yeganeh, S., Keramat Amirkolaie, A., 2017. Effect of sodium selenite on the bacteria growth, selenium accumulation, and selenium biotransformation in *Pediococcus acidilactici*. Food Sci. Biotechnol. 26, 1013–1018. https://doi.org/10.1007/s10068-017-0142-y.

Li, D.-B., Cheng, Y.-Y., Wu, C., Li, W.-W., Li, N., Yang, Z.-C., Tong, Z.-H., Yu, H.-Q., 2014. Selenite reduction by *Shewanella oneidensis* MR-1 is mediated by fumarate reductase in periplasm. Sci. Rep. 4, 1–7. https://doi.org/10.1038/srep03735.

Lopez-Fernandez, M., Fernández-Sanfrancisco, O., Moreno-García, A., Martín-Sánchez, I., Sánchez-Castro, I., Merroun, M.L., 2014. Microbial communities in bentonite formations and their interactions with uranium. Appl. Geochem. 49, 77–86. https://doi.org/10.1016/j.apgeochem.2014.06.022.

Lopez-Fernandez, M., Cherkouk, A., Vilchez-Vargas, R., Jauregui, R., Pieper, D., Boon, N., Sanchez-Castro, I., Merroun, M.L., 2015. Bacterial Diversity in Bentonites, Engineered Barrier for Deep Geological Disposal of Radioactive Wastes. Micro Ecol. 70, 922–935. https://doi.org/10.1007/s00248-015-0630-7.

Lopez-Fernandez, M., Vilchez-Vargas, R., Jroundi, F., Boon, N., Pieper, D., Merroun, M. L., 2018. Microbial community changes induced by uranyl nitrate in bentonite clay microcosms. Appl. Clay Sci., ACS - SI ICC 2017 XVI Int. Clay Conf. – Clays, Oceans Space 160, 206–216. https://doi.org/10.1016/j.clay.2017.12.034.

Lucovsky, G., Mooradian, A., Taylor, W., Wright, G.B., Keezer, R.C., 1967. Identification of the fundamental vibrational modes of trigonal, α - monoclinic and amorphous selenium. Solid State Commun. 5, 113–117. https://doi.org/10.1016/0038-1098(67)90006-3.

Montavon, G., Guo, Z., Lützenkirchen, J., Alhajji, E., Kedziorek, M.A.M., Bourg, A.C.M., Grambow, B., 2009. Interaction of selenite with MX-80 bentonite: Effect of minor phases, pH, selenite loading, solution composition and compaction. Colloids Surf. A: Physicochem. Eng. Asp. 332, 71–77. https://doi.org/10.1016/j.colsurfa.2008.09.014.

Nagata, K., Ishibashi, K., Miyamoto, Y., 1981. Raman and infrared spectra of rhombohedral selenium. Jpn. J. Appl. Phys. 20, 463. https://doi.org/10.1143/JJAP.20.463.

Nancharaiah, Y.V., Lens, P.N.L., 2015. Ecology and biotechnology of selenium-respiring bacteria. Microbiol. Mol. Biol. Rev. 79, 61–80. https://doi.org/10.1128/MMBR.00037-14.

Oremland, R.S., Herbel, M.J., Blum, J.S., Langley, S., Beveridge, T.J., Ajayan, P.M., Sutto, T., Ellis, A.V., Curran, S., 2004. Structural and Spectral Features of Selenium Nanospheres Produced by Se-Respiring Bacteria. Appl. Environ. Microbiol 70, 52–60. https://doi.org/10.1128/AEM.70.1.52-60.2004.

Patil, Y., Junghare, M., Müller, N., 2016. Fermentation of glycerol by *Anaerobium acetethylicum* and its potential use in biofuel production. Micro Biotechnol. 10, 203–217. https://doi.org/10.1111/1751-7915.12484.

Pinel-Cabello, M., Chapon, V., Ruiz-Fresneda, M.A., Alpha-Bazin, B., Berthomieu, C., Armengaud, J., Merroun, M.L., 2021. Delineation of cellular stages and identification of key proteins for reduction and biotransformation of Se(IV) by *Stenotrophomonas bentonitica* BII-R7. J. Hazard. Mater. 418, 126150 https://doi.org/10.1016/j.jhazmat.2021.126150.

Povedano-Priego, C., Jroundi, F., Lopez-Fernandez, M., Sánchez-Castro, I., Martin-Sánchez, I., Huertas, F.J., Merroun, M.L., 2019. Shifts in bentonite bacterial community and mineralogy in response to uranium and glycerol-2-phosphate exposure. Sci. Total Environ. 692, 219–232. https://doi.org/10.1016/j.scitotenv.2019.07.228.

Povedano-Priego, C., Jroundi, F., Lopez-Fernandez, M., Shrestha, R., Spanek, R., Martín-Sánchez, I., Villar, M.V., Ševců, A., Dopson, M., Merroun, M.L., 2021. Deciphering indigenous bacteria in compacted bentonite through a novel and efficient DNA extraction method: Insights into biogeochemical processes within the Deep Geological Disposal of nuclear waste concept. J. Hazard. Mater. 408, 124600 https://doi.org/10.1016/j.jhazmat.2020.124600.

Povedano-Priego, C., Jroundi, F., Lopez-Fernandez, M., Morales-Hidalgo, M., Martin-Sánchez, I., Huertas, F.J., Dopson, M., Merroun, M.L., 2022. Impact of anoxic conditions, uranium(VI) and organic phosphate substrate on the biogeochemical potential of the indigenous bacterial community of bentonite. Appl. Clay Sci. 216, 106331 https://doi.org/10.1016/j.clay.2021.106331.

Ravel, B., Newville, M., 2005. ATHENA, ARTEMIS, HEPHAESTUS: data analysis for X-ray absorption spectroscopy using IFEFFIT. J. Synchrotron Rad. 12, 537–541. https://doi.org/10.1107/S0909049505012719.

Robertson, C.E., Harris, J.K., Wagner, B.D., Granger, D., Browne, K., Tatem, B., Feazel, L. M., Park, K., Pace, N.R., Frank, D.N., 2013. Explicet: graphical user interface software for metadata-driven management, analysis and visualization of microbiome data. Bioinformatics 29, 3100–3101. https://doi.org/10.1093/bioinformatics/btt526.

Rosenfeld, C.E., James, B.R., Santelli, C.M., 2018. Persistent Bacterial and Fungal Community Shifts Exhibited in Selenium-Contaminated Reclaimed Mine Soils. Appl. Environ. Microbiol 84. https://doi.org/10.1128/AEM.01394-18.

Ruiz-Fresneda, M.A., Martín, J.D., Bolívar, J.G., Cantos, M.V.F., Bosch-Estévez, G., Moreno, M.F.M., Merroun, M.L., 2018. Green synthesis and biotransformation of amorphous Se nanospheres to trigonal 1D Se nanostructures: impact on Se mobility within the concept of radioactive waste disposal. Environ. Sci.: Nano 5, 2103–2116. ⟨https://doi.org/10.1039/C8EN00221E⟩.

Ruiz-Fresneda, M.A., Gomez-Bolivar, J., Delgado-Martin, J., Abad-Ortega, M., del, M., Guerra-Tschuschke, I., Merroun, M.L., 2019. The Bioreduction of Selenite under Anaerobic and Alkaline Conditions Analogous to Those Expected for a Deep Geological Repository System. Molecules 24, 3868. https://doi.org/10.3390/molecules24213868.

Ruiz-Fresneda, M.A., Eswayah, A.S., Romero-González, M., Gardiner, P.H.E., Solari, P.L., Merroun, M.L., 2020. Chemical and structural characterization of SeIV biotransformations by *Stenotrophomonas bentonitica* into Se0 nanostructures and volatiles Se species. Environ. Sci.: Nano 7, 2140–2155. https://doi.org/10.1039/D0EN00507J.

Sánchez-Castro, I., Ruiz-Fresneda, M.A., Bakkali, M., Kämpfer, P., Glaeser, S.P., Busse, H. J., López-Fernández, M., Martínez-Rodríguez, P., Merroun, M.L., 2017. *Stenotrophomonas bentonitica* sp. nov., isolated from bentonite formations. Int. J. Syst. Evol. Microbiol 67, 2779–2786. https://doi.org/10.1099/ijsem.0.002016.

Sarret, G., Avoscan, L., Carrière, M., Collins, R., Geoffroy, N., Carrot, F., Covès, J., Gouget, B., 2005. Chemical forms of selenium in the metal-resistant bacterium *Ralstonia metallidurans* CH34 exposed to selenite and selenate. Appl. Environ. Microbiol. 71, 2331–2337. https://doi.org/10.1128/AEM.71.5.2331-2337.2005.

Shiratori-Takano, H., Akita, K., Yamada, K., Itoh, T., Sugihara, T., Beppu, T., Ueda, K., 2014. Description of *Symbiobacterium ostreiconchae* sp. nov., *Symbiobacterium turbinis* sp. nov. and *Symbiobacterium terraclitae* sp. nov., isolated from shellfish, emended description of the genus *Symbiobacterium* and proposal of *Symbiobacteriaceae* fam. nov. Int. J. Syst. Evolut. Microbiol. 64, 3375–3383. https://doi.org/10.1099/ijs.0.063750-0.

Sitaud, B., Solari, P.L., Schlutig, S., Llorens, I., Hermange, H., 2012. Characterization of radioactive materials using the MARS beamline at the synchrotron SOLEIL. J. Nucl. Mater., Microstruct. Prop. Irradiat. Mater. 425, 238–243. https://doi.org/10.1016/j.jnucmat.2011.08.017.

Solari, P.L., Schlutig, S., Hermange, H., Sitaud, B., 2009. MARS, a new beamline for radioactive matter studies at SOLEIL. J. Phys.: Conf. Ser. 190, 012042 https://doi.org/10.1088/1742-6596/190/1/012042.

de Souza, M.P., Chu, D., Zhao, M., Zayed, A.M., Ruzin, S.E., Schichnes, D., Terry, N., 1999. Rhizosphere Bacteria Enhance Selenium Accumulation and Volatilization by Indian Mustard. Plant Physiol. 119, 565–574.

Tam, K., Ho, C.T., Lee, J.-H., Lai, M., Chang, C.H., Rheem, Y., Chen, W., Hur, H.-G., Myung, N.V., 2010. Growth mechanism of amorphous selenium nanoparticles synthesized by *Shewanella* sp. HN-41. Biosci. Biotechnol. Biochem. 74, 696–700. https://doi.org/10.1271/bbb.90454.

Urík, M., Bujdoš, M., Gardošová, K., Littera, P., Matúš, P., 2018. Selenite distribution in multicomponent system consisting of filamentous fungus, humic acids, bentonite, and ferric oxyhydroxides. Water Air Soil Pollut. 229, 52. https://doi.org/10.1007/s11270-018-3719-z.

Wang, T., Yang, L., Zhang, B., Liu, J., 2010. Extracellular biosynthesis and transformation of selenium nanoparticles and application in H_2O_2 biosensor. Colloids Surf. B: Biointerfaces 80, 94–102. https://doi.org/10.1016/j.colsurfb.2010.05.041.

Wang, Z., Wang, Y., Gomes, R.L., Gomes, H.I., 2022. Selenium (Se) recovery for technological applications from environmental matrices based on biotic and abiotic mechanisms. J. Hazard. Mater. 427, 128122 https://doi.org/10.1016/j.jhazmat.2021.128122.

Wells, M., McGarry, J., Gaye, M.M., Basu, P., Oremland, R.S., Stolz, J.F., 2019. Respiratory Selenite Reductase from *Bacillus selenitireducens* Strain MLS10. J. Bacteriol. 201. https://doi.org/10.1128/JB.00614-18.

Xiao, Y., Francke, C., Abee, T., Wells-Bennik, M.H.J., 2011. Clostridial spore germination versus bacilli: Genome mining and current insights. Food Microbiol. 28, 266–274. https://doi.org/10.1016/j.fm.2010.03.016.

Xu, W., Qin, H.-B., Zhu, J.-M., Johnson, T.M., Tan, D., Liu, C., Takahashi, Y., 2021. Selenium isotope fractionation during adsorption onto montmorillonite and kaolinite. Appl. Clay Sci. 211, 106189 https://doi.org/10.1016/j.clay.2021.106189.

Yang, S., Li, S., Jia, X., 2019. Production of medium chain length polyhydroxyalkanoate from acetate by engineered *Pseudomonas putida* KT2440. J. Ind. Microbiol Biotechnol. 46, 793–800. https://doi.org/10.1007/s10295-019-02159-5.

Zhao, Y.H., Lu, K., Liu, T., 2004. EXAFS study of mechanical-milling-induced solid-state amorphization of Se. J. Non-Cryst. Solids 356, 246–251. https://doi.org/10.1016/j.jnoncrysol.2003.12.055.